



PERGAMON

Journal of the Mechanics and Physics of Solids
50 (2002) 1591–1625

JOURNAL OF THE
MECHANICS AND
PHYSICS OF SOLIDS

www.elsevier.com/locate/jmps

Some surprising phenomena in weak-bond fracture of a triangular lattice

L.I. Slepyan^{a,*}, M.V. Ayzenberg-Stepanenko^b

^a*Department of Solid Mechanics, Materials and Systems, Faculty of Engineering, Tel Aviv University, P.O. Box 39040, Ramat Aviv 69978 Tel Aviv, Israel*

^b*Department of Mathematics, Ben-Gurion University of the Negev, Beer Sheva 84205, Israel*

Received 2 August 2001; received in revised form 27 November 2001; accepted 10 December 2001

Abstract

A semi-infinite crack growing along a straight line in an unbounded triangular-cell lattice and in lattice strips is under examination. Elastic and standard-material viscoelastic lattices are considered. Using the superposition similar to that used for a square-cell lattice (J. Mech. Phys. Solids 48 (2000) 927) an irregular stress distribution is revealed on the crack line in mode II: the strain of the crack-front bond is lower than that of the next bond. A further notable fact about mode II concerns the bonds on the crack line in the lattice strip deformed by a 'rigid machine'. If the alternate bonds, such that are inclined differently than the crack-front bond, are removed, the stresses in the crack-front bond and in the other intact bonds decrease. These facts result in irregular quasi-static and dynamic crack growth. In particular, in a wide range of conditions for mode II, consecutive bond breaking becomes impossible. The most surprising phenomenon is the formation of a *binary crack* consisting of two branches propagating on the same line. It appears that the consecutive breaking of the right-slope bonds—as one branch of the crack—can proceed at a speed different from that for the left-slope bonds—as another branch. One of these branches can move faster than the other, but with time they can change places. Some irregularities are observed in mode I as well. Under the influence of viscosity, crack growth can be stabilized and crack speed can be low when viscosity is high; however, in mode II irregularities in the crack growth remain. It is found that crack speed is a discontinuous function of the creep and relaxation times. © 2002 Elsevier Science Ltd. All rights reserved.

Keywords: A. Fracture; B. Viscoelastic lattice; C. Integral transforms

* Corresponding author. Tel.: +972-3640-6224; fax: +972-3640-7617.
E-mail address: leonid@eng.tau.ac.il (L.I. Slepyan).

1. Introduction

Analytical solutions for crack propagation in a plane triangular-cell lattice were derived for uniform straight line crack growth, that is, these solutions correspond to the cutting of crack-path bonds with a given speed. The first work along these lines was published by Kulakhmetova et al. (1984) where the total dissipation was found for the case of a sub-Rayleigh macrolevel-associated solution. Recently, the complete set of the macrolevel-associated and the microlevel solutions for all crack speed regimes, sub-Rayleigh, super-Rayleigh, intersonic and supersonic ones, was considered by Slepyan (2001). Stability of crack propagation in this lattice was examined by Marder and Liu (1993), Marder and Gross (1995) and Fineberg and Marder (1999). Also, Kelvin-type viscoelastic square and triangular lattices were considered by Kessler and Levine (1998, 2000), Kessler (1999) and Pechenik et al. (2000a,b). A square-cell lattice made of a standard viscoelastic material was examined by Slepyan et al. (1999). In these works, if numerical simulations of the lattice fracture were performed, the crack path and the crack velocity were not prescribed in advance.

Note that mode II fracture admits intersonic crack propagation. This regime for an elastic homogeneous material was considered in a number of works, in particular, in Burrige et al. (1979), Freund (1979), Slepyan (1981), Broberg (1999), Gao et al. (1999). Numerical simulations and experiments also show the possibility of intersonic crack propagation (Rosakis et al., 1998, 1999; Needleman and Rosakis, 1999; Abraham and Gao, 2000). Mode II for the triangular-cell lattice was recently considered by Gerde and Marder (2001) and Slepyan (2001).

If slow crack growth in a discrete lattice is considered, the dynamic amplification factor can be found to play a crucial role in the process. For a stressed lattice with a growing crack the question whether the crack can propagate slowly can be answered based on the examination of an auxiliary transient problem as follows. Consider a lattice with a crack whose faces are subjected to a suddenly applied self-equilibrated pair of forces as in Fig. 2 (this transient problem is considered below). When the forces are applied, the strain of the first intact bond rises and develops tending to the corresponding static value. If the strain approaches the static value but remains below it at all times, the crack can grow slowly. Otherwise—in the case of the dynamic factor manifestation—slow crack growth is impossible. This phenomenon was recently studied based on mode III fracture in a square-cell lattice (Slepyan, 2000).

In the present paper, the role of the dynamic factor in modes I and II fracture of the triangular-cell lattice is examined. It is of interest that in this study, an attempt to extend the analysis to mode II has immediately led to an unexpected conclusion. It appears that in statics the strain of the crack-front bond is lower than that of the next bond. A further notable fact about mode II concerns the bonds on the crack line in the lattice strip deformed by a ‘rigid machine’. If the alternate bonds, such that are inclined differently than the crack-front bond, are removed, the stresses in the crack-front bond and in the other intact bonds decrease. Although in the case of mode I the crack-tip bond is stressed higher than the next one and the following, an irregular dependence of the stress on the bond number is observed as well. These facts suggest uncommon dynamic behavior of the crack and this is really observed in the numerical simulations

where the crack propagation in elastic and viscoelastic triangular-cell lattice strip is then under examination.

In the present work, some analytical examination of the triangular lattice with a semi-infinite crack is followed by numerical simulations where the crack path is prescribed to be a straight line, but the time-dependent crack speed is not prescribed in advance; instead a limiting elongation fracture criterion is used. Such a straight-line crack growth can occur, in particular, in the case where the bonds on the crack path are weaker than those outside. Note that weak-bond fracture was examined by Ravi-Chandar and Knauss (1984) and Lee and Knauss (1989).

This formulation enables some uncommon fracture phenomena to be observed. The most surprising dynamic phenomenon arising in mode II is the formation of a *binary crack* consisting of two branches growing along the same line. It appears that the consecutive breaking of the right-slope bonds proceeds at a speed different from that for the left-bend bonds. It looks as if these two branches of the binary crack are weakly connected with each other. One of them can move faster than the other, but with time they can change places. This and some other uncommon phenomena are discussed below. In the examination of the role of viscosity in the crack propagation, it is found in particular that crack speeds are discontinuous functions of the creep and relaxation times. Also, it is learned how viscosity influences the dynamic factor.

2. The lattice

We consider static and transient crack problems for elastic and viscoelastic triangular-cell lattices and lattice strips. Geometrically, the lattice is the same as the elastic lattice in Slepyan (2001), where steady-state crack propagation was examined. Note that a square-cell viscoelastic lattice was considered in Slepyan et al. (1999) and Slepyan (2000).

In the triangular lattice (Fig. 1(a)), each particle of mass M is connected with six neighbors by the same bonds, each of the length a and the static stiffness E . Coordinates

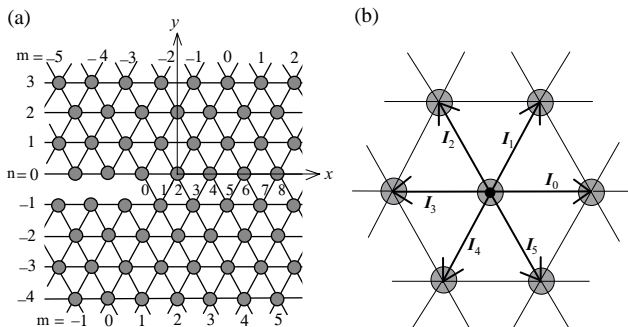


Fig. 1. The lattice: (a) the lattice and the coordinates, (b) the unit vectors.

of the particles are defined by the position vector

$$\mathbf{x}' = m\mathbf{I}_0 + n\mathbf{I}_1, \tag{1}$$

where m and n are integer numbers, and $\mathbf{I}_p, p=0, 1, \dots, 5$, are the unit vectors directed from a given particle to the neighboring ones (Fig. 1(b)). In terms of the projections onto x -, y -axis shown in Fig. 1(a) these vectors are

$$\mathbf{I}_p = [\cos(\pi p/3), \sin(\pi p/3)]. \tag{2}$$

In addition, we introduce unit vectors \mathbf{I}_x and \mathbf{I}_y directed along the x - and y -axis, respectively. Therefore, we may use both the rectangular coordinates, $x = m + n/2$, $y = \sqrt{3}n/2$, and the m, n -system.

The crack faces are formed by particles with $n = 0$ and -1 . We denote the bond elongation (or the lengthening of the distance between the corresponding particles) by $Q_p(t, m, n)$:

$$\begin{aligned} Q_0(t, m, n) &= [\mathbf{u}(t, m + 1, n) - \mathbf{u}(t, m, n)]\mathbf{I}_0, \\ Q_1(t, m, n) &= [\mathbf{u}(t, m, n + 1) - \mathbf{u}(t, m, n)]\mathbf{I}_1, \\ Q_2(t, m, n) &= [\mathbf{u}(t, m - 1, n + 1) - \mathbf{u}(t, m, n)]\mathbf{I}_2, \\ Q_3(t, m, n) &= [\mathbf{u}(t, m - 1, n) - \mathbf{u}(t, m, n)]\mathbf{I}_3, \\ Q_4(t, m, n) &= [\mathbf{u}(t, m, n - 1) - \mathbf{u}(t, m, n)]\mathbf{I}_4, \\ Q_5(t, m, n) &= [\mathbf{u}(t, m + 1, n - 1) - \mathbf{u}(t, m, n)]\mathbf{I}_5. \end{aligned} \tag{3}$$

The corresponding bond is denoted by $B_p(m, n)$ and the tensile force in this bond is denoted as $T_p(t, m, n)$.

The bonds are assumed to obey a standard viscoelastic law. In terms of the Laplace transform with parameter s , the connection between the internal tensile force and elongation of an intact bond is

$$T_p^L(s, m, n) = E\hat{E}Q_p^L(s, m, n), \quad \hat{E} = \frac{1 + \alpha s}{1 + \beta s}, \tag{4}$$

where α and β are creep and relaxation times, respectively, and E is the elastic stiffness.

In the long-wave approximation, the lattice corresponds to a two-dimensional, homogeneous, isotropic, viscoelastic body with density $\rho = 2M/(\sqrt{3}a^2)$, Poisson's ratio $\nu = 1/3$ and the complex stiffness $E\hat{E}$. The following velocities of the longitudinal, shear and Rayleigh waves correspond to the slow-process stiffness ($\hat{E} = 1$): $c_1 = \sqrt{9/8}c$, $c_2 = \sqrt{3/8}c$ and $c_R = \frac{1}{2}\sqrt{3 - \sqrt{3}}c$, respectively, where $c = a\sqrt{E/M}$. The shear modulus is $\mu = \rho c_2^2 = \sqrt{3}E/4$.

In the following, we use nondimensional values associated with the natural units: the particle mass ($M = 1$), the bond length ($a = 1$) and the bond static stiffness ($E = 1$). In these terms, c is the speed unit ($c = 1$), a/c is the time unit, $\rho = 2/\sqrt{3}$, $c_1 = \sqrt{9/8}$, $c_2 = \sqrt{3/8}$ and $c_R = \frac{1}{2}\sqrt{3 - \sqrt{3}}$.

At the moment when the strain first exceeds a critical value, Q_* , the bond is assumed to disappear.

3. Superposition

As in the paper on a square-cell lattice (Slepyan, 2000) consider two problems. The first is the main problem for a homogeneous static state of a lattice stressed by remote forces. The lattice contains a crack such that the bond $B_5(-1,0)$ exists as the crack front, and the bonds $B_4(m,0)$ and $B_5(m,0), m \geq 0$, are also intact, while the bond $B_4(-1,0)$ and all the bonds at the left, $B_5(m,0)$ and $B_4(m,0), m \leq -2$ do not exist (Fig. 1(a)). Let us enumerate the crack-path bonds ahead of the crack beginning from the crack-front bond $B_5(-1,0)$ as shown in Fig. 1(a)

$$B_0 = B_5(-1,0), \quad B_1 = B_4(0,0), \quad B_2 = B_5(0,0), \dots \tag{5}$$

and the respective tensile forces as

$$T_0(t) = T_5(t, -1, 0), \quad T_1(t) = T_4(t, 0, 0), \quad T_2(t) = T_5(t, 0, 0), \dots, \tag{6}$$

where we take $t = 0$ for this static problem. Note that in the elastic case the nondimensional tensile force and the respective elongation of any intact bond are equal to each other, $T_j(t) = Q_j(t)$ (we use the same numbering for the crack-path elongation as for the tensile force).

The second is an auxiliary dynamic problem for the same, but initially unstressed lattice with the crack extended due to the destruction of the zero bond, B_0 . This lattice, being initially at rest, at $t = 0$ is suddenly loaded by the force $\mathbf{P} = T_0(0)\mathbf{I}_2$ applied to the particle with $m = -1, n = 0$, and the same but opposite force, $T_0(0)\mathbf{I}_5$, applied to the particle with $m = 0, n = -1$, Fig. 2. Let us denote the tensile forces on the crack line in this auxiliary problem by $T_j^+(t)T_0(0)$. Note that the functions $T_j^+(t)$ are independent of $T_0(0)$ since a linear problem is considered.

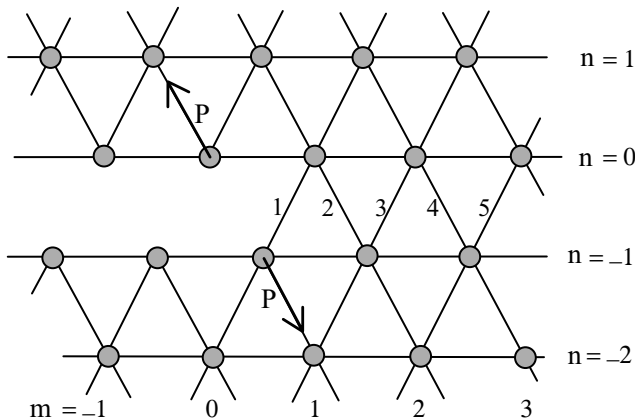


Fig. 2. Forces in the auxiliary problem.

Further consider the resulting problem. It corresponds to the first one where the crack-front bond B_0 disappears at $t = 0$ because the total crack-face forces corresponding to this bond are zero for $t > 0$. This problem relates to very slow crack growth when the time interval between the destruction of neighboring bonds is large enough to permit the lattice to approach the static state before the next bond is broken.

The tensile forces in the intact bonds are thus

$$T_j(t) = T_j(0) + T_j^+(t)T_0(0) \quad (j \geq 1). \tag{7}$$

For the final static state we thus have

$$T_j(\infty) = T_j(0) + T_j^+(\infty)T_0(0) \quad (j \geq 1). \tag{8}$$

3.1. Superposition paradox

In the considered homogeneous static problem, after the bond B_0 is removed the distribution of the tensile forces relative to the crack front remains completely the same in the case of mode I and only changes sign in the case of mode II. This follows directly from symmetry of the lattice. Thus,

$$\begin{aligned} T_j(\infty) &= T_{j-1}(0) \quad (\text{mode I}), \\ T_j(\infty) &= -T_{j-1}(0) \quad (\text{mode II}). \end{aligned} \tag{9}$$

Referring to Eq. (8) we get

$$\begin{aligned} T_1(0) &= T_0(0)[1 - T_1^+(\infty)] \quad (\text{mode I}), \\ T_1(0) &= -T_0(0)[1 + T_1^+(\infty)] \quad (\text{mode II}). \end{aligned} \tag{10}$$

We face a paradoxical result: in one of these two modes the tensile force in the second bond is higher than that in the crack front bond. So, if the tensile force $T_0(0)$ in mode I is maximal at the crack front, $T_1(0) < T_0(0)$, then $T_1^+(\infty) > 0$ and for mode II the opposite inequality is true:

$$|T_1(0)| > |T_0(0)|. \tag{11}$$

Otherwise, if one expects that $T_1^+(\infty) < 0$, the last conclusion is valid for mode I.

As shown below, $T_1^+(\infty) > 0$ and hence a surprising result arises for mode II. In fact, the tensile force in the second bond ($j = 1$) appears to be equal to $-5/4$ of that for the first one ($j = 0$). Thus, if mode II fracture for the lattice stressed by remote forces is considered, the second bond must break before the first one. Note that in the case of different limits for extension and compression, this irregular mode of fracture will at least alternate with the regular one during the crack growth.

4. Transient problem for an intact viscoelastic lattice

4.1. Equations and transformations

The dynamic equation for a particle is

$$\begin{aligned} & \left(1 + \beta \frac{d}{dt}\right) \frac{d^2 \mathbf{u}(t, m, n)}{dt^2} - \left(1 + \alpha \frac{d}{dt}\right) \sum_{p=0}^5 Q_p(t, m, n) \mathbf{I}_p \\ & = \left(1 + \beta \frac{d}{dt}\right) \sum_{p=0}^5 P_p(t, m, n) \mathbf{I}_p, \end{aligned} \tag{12}$$

where P_p are external forces and, as already noted, α and β are creep and relaxation times, respectively. In terms of the Laplace transform

$$\mathbf{u}^L(s, m, n) = \int_0^\infty \mathbf{u}(t, m, n) e^{-st} dt \tag{13}$$

the equation is

$$s^2 \mathbf{u}^L(s, m, n) - \hat{E} \sum_{p=0}^5 Q_p^L(s, m, n) \mathbf{I}_p = \sum_{p=0}^5 P_p^L(s, m, n) \mathbf{I}_p, \quad \hat{E} = \frac{1 + \alpha s}{1 + \beta s}. \tag{14}$$

Further, we use the double discrete Fourier transform with respect to m and n

$$\mathbf{u}^{\text{LFF}}(s, k, q) = \sum_{m=-\infty}^\infty \sum_{n=-\infty}^\infty \mathbf{u}^L(s, m, n) \exp[i(km + qn)]. \tag{15}$$

We get

$$s^2 \mathbf{u}^{\text{LFF}}(s, k, q) - \hat{E} \sum_{p=0}^5 Q_p^{\text{LFF}}(s, k, q) \mathbf{I}_p = \sum_{p=0}^5 P_p^{\text{LFF}}(s, k, q) \mathbf{I}_p. \tag{16}$$

In the following, the external forces are assumed to be applied only to lines $n = 0$ and -1 as

$$P_1(t, m, 0) \mathbf{I}_1, \quad P_2(t, m, 0) \mathbf{I}_2, \quad P_4(t, m, -1) \mathbf{I}_4, \quad P_5(t, m, -1) \mathbf{I}_5 \tag{17}$$

with

$$P_4(t, m, -1) = P_1(t, m, 0), \quad P_5(t, m, -1) = P_2(t, m - 1, 0), \tag{18}$$

that is, these forces are self-equilibrated. In this case, Eq. (16) becomes

$$\begin{aligned} & s^2 \mathbf{u}^{\text{LFF}}(s, k, q) - \hat{E} \sum_{p=0}^5 Q_p^{\text{LFF}}(s, k, q) \mathbf{I}_p \\ & = (\mathbf{I}_1 + e^{-iq} \mathbf{I}_4) P_1^{\text{LF}}(s, k, 0) + (\mathbf{I}_2 + e^{i(k-q)} \mathbf{I}_5) P_2^{\text{LF}}(s, k, 0) \\ & = (1 - e^{-iq}) P_1^{\text{LF}}(s, k, 0) \mathbf{I}_1 + (1 - e^{i(k-q)}) P_2^{\text{LF}}(s, k, 0) \mathbf{I}_2. \end{aligned} \tag{19}$$

The x, y -projections of this equation are

$$\begin{aligned}
 s^2 u_x^{\text{LFF}}(s, k, q) - \hat{E} \sum_{p=0}^5 Q_p^{\text{LFF}}(s, k, q) \mathbf{I}_p \mathbf{I}_x \\
 = \frac{1}{2} [(1 - e^{-iq}) P_1^{\text{LF}}(s, k, 0) - (1 - e^{i(k-q)}) P_2^{\text{LF}}(s, k, 0)], \\
 s^2 u_y^{\text{LFF}}(s, k, q) - \hat{E} \sum_{p=0}^5 Q_p^{\text{LFF}}(s, k, q) \mathbf{I}_p \mathbf{I}_y \\
 = \frac{\sqrt{3}}{2} [(1 - e^{-iq}) P_1^{\text{LF}}(s, k, 0) + (1 - e^{i(k-q)}) P_2^{\text{LF}}(s, k, 0)]
 \end{aligned} \tag{20}$$

with

$$\begin{aligned}
 Q_0^{\text{LFF}}(s, k, q) &= (e^{-ik} - 1) \mathbf{u}^{\text{LFF}}(s, k, q) \mathbf{I}_0, \\
 Q_1^{\text{LFF}}(s, k, q) &= (e^{-iq} - 1) \mathbf{u}^{\text{LFF}}(s, k, q) \mathbf{I}_1, \\
 Q_2^{\text{LFF}}(s, k, q) &= (e^{i(k-q)} - 1) \mathbf{u}^{\text{LFF}}(s, k, q) \mathbf{I}_2, \\
 Q_3^{\text{LFF}}(s, k, q) &= (e^{ik} - 1) \mathbf{u}^{\text{LFF}}(s, k, q) \mathbf{I}_3, \\
 Q_4^{\text{LFF}}(s, k, q) &= (e^{iq} - 1) \mathbf{u}^{\text{LFF}}(s, k, q) \mathbf{I}_4, \\
 Q_5^{\text{LFF}}(s, k, q) &= (e^{-i(k-q)} - 1) \mathbf{u}^{\text{LFF}}(s, k, q) \mathbf{I}_5
 \end{aligned} \tag{21}$$

and

$$\mathbf{I}_p \mathbf{I}_x = \cos(\pi p/3), \mathbf{I}_p \mathbf{I}_y = \sin(\pi p/3). \tag{22}$$

We come to the following equations:

$$\begin{aligned}
 [Y + 1 + 4 \sin^2 k/2 - \cos k/2 \cos(q - k/2)] u_x^{\text{LFF}}(s, k, q) \\
 + \sqrt{3} \sin k/2 \sin(q - k/2) u_y^{\text{LFF}}(s, k, q) \\
 = \frac{1}{2\hat{E}} [(1 - e^{-iq}) P_1^{\text{LF}}(s, k, 0) - (1 - e^{i(k-q)}) P_2^{\text{LF}}(s, k, 0)], \\
 \sqrt{3} \sin k/2 \sin(q - k/2) u_x^{\text{LFF}}(s, k, q) \\
 + [Y + 3(1 - \cos k/2 \cos(q - k/2))] u_y^{\text{LFF}}(s, k, q) \\
 = \frac{\sqrt{3}}{2\hat{E}} [(1 - e^{-iq}) P_1^{\text{LF}}(s, k, 0) + (1 - e^{i(k-q)}) P_2^{\text{LF}}(s, k, 0)],
 \end{aligned} \tag{23}$$

where $Y = s^2/\hat{E}$. From this and Eqs. (21) it follows that

$$\begin{aligned}
 Q_4^{\text{LFF}} = \frac{1}{\Delta} \{2(1 - \cos q)[2Y + 6 \sin^2 k/2 + 3(1 - \cos(q - k))] P_1^{\text{LF}}(s, k, 0) \\
 + (e^{iq} - 1)(e^{i(k-q)} - 1)(Y + 6 \sin^2 k/2) P_2^{\text{LF}}(s, k, 0)\},
 \end{aligned}$$

$$Q_5^{\text{LFF}} = \frac{1}{A} \{ (e^{-iq} - 1)(e^{-i(k-q)} - 1)(Y + 6 \sin^2 k/2) P_1^{\text{LF}}(s, k, 0) + 2[1 - \cos(q - k)][2Y + 6 \sin^2 k/2 + 3(1 - \cos q)] P_2^{\text{LF}}(s, k, 0) \},$$

$$A = 6\hat{E}[(n_1 - \cos(q - k/2))(n_2 - \cos(q - k/2))], \tag{24}$$

where

$$n_1 = b - \sqrt{b^2 - d}, \quad n_2 = b + \sqrt{b^2 - d},$$

$$b = (1 + 2 \sin^2 k/2 + \frac{2}{3}Y) \cos k/2,$$

$$d = 1 + 3 \sin^2 k/2 + \frac{1}{3}Y(4 + 4 \sin^2 k/2 + Y),$$

$$b^2 - d = \frac{1}{9} Y^2 - 4 \sin^2 \frac{k}{2} \left(\sin^2 \frac{k}{2} + \frac{1}{3} Y \right)^2. \tag{25}$$

4.2. Fundamental solution

Let us introduce a combination of the functions, Q_4^{LFF} and Q_5^{LFF} , as

$$Q^{\text{LFF}}(s, k, q) = Q_4^{\text{LFF}}(s, k, q) + e^{ik/2} Q_5^{\text{LFF}}(s, k, q). \tag{26}$$

Now consider the inverse Fourier transform with respect to q for $n = 0$

$$Q^{\text{LF}}(s, k, 0) = \frac{1}{2\pi} \int_{-\pi}^{\pi} Q^{\text{LFF}}(s, k, q) dq. \tag{27}$$

In this integral, one can substitute $q = q' + k/2$. Since the integrand is a 2π -periodic function of q , the integration limits can be retained. As a result, one obtains

$$Q^{\text{LF}}(s, k, 0) = \frac{1}{2\pi} \int_{-\pi}^{\pi} S(s, k, q) \mathcal{P}^{\text{LF}}(s, k) dq, \tag{28}$$

where

$$\mathcal{P}^{\text{LF}}(s, k) = P_1^{\text{LF}}(s, k, 0) + e^{ik/2} P_2^{\text{LF}}(s, k, 0) \tag{29}$$

and

$$S = \frac{1}{A_0} [3(\cos k/2 - \cos q)^2 + 2(1 - \cos k/2 \cos q)(Y + 3 \sin^2 k/2) + (\cos k/2 - \cos q)(Y + 6 \sin^2 k/2)],$$

$$A_0 = 3\hat{E}(n_1 - \cos q)(n_2 - \cos q). \tag{30}$$

Note that S is a regular function of q for $\Im k = 0, Y > 0$, since under these conditions $n_{1,2}^2 > 1$ if $\Im n_{1,2} = 0$.

We come to the following fundamental solution:

$$Q^{LF}(s, k, 0) = \frac{1}{\hat{E}} [1 - 1/L(s, k)] \mathcal{P}^{LF}(s, k),$$

$$L(s, k) = \frac{3(n_1 - n_2)\sqrt{n_1^2 - 1}\sqrt{n_2^2 - 1}}{(\phi + \psi n_1)\sqrt{n_2^2 - 1} - (\phi + \psi n_2)\sqrt{n_1^2 - 1}}$$

$$= \frac{3\sqrt{n_1^2 - 1}\sqrt{n_2^2 - 1}(\sqrt{n_1^2 - 1} + \sqrt{n_2^2 - 1})}{\psi\sqrt{n_2^2 - 1}(\sqrt{n_1^2 - 1} + \sqrt{n_2^2 - 1}) - (\phi + \psi n_2)(n_1 + n_2)},$$

$$\phi = Y \cos k/2 - 6(1 - \cos k/2) \sin^2 k/2 + 4Y \cos^2 k/2 - 6Y - Y^2,$$

$$\psi = 2Y \cos k/2 - 6(1 - \cos k/2) \sin^2 k/2 - Y. \tag{31}$$

5. Lattice with a crack

5.1. Governing equation

Let us represent

$$\mathcal{P}^{LF}(s, k) = \hat{E}Q_-(s, k) + P^{LF}(s, k), \tag{32}$$

where

$$Q_-(s, k) = Q^{LF}(s, k, 0) - Q_+(s, k) = \sum_{m=-\infty}^{-1} Q^L(s, m, 0) \tag{33}$$

and $P^{LF}(s, k)$ is the double transform of the rest of the external forces. We now come to a solution for the lattice with a crack, that is the lattice without bonds $B_4(m, 0)$ and $B_5(m, 0)$ for $m < 0$ (Fig. 2), since their action on the lattice is compensated by the first term on the right-hand side of Eq. (32). We obtain the governing equation as

$$L(s, k)Q_+ + Q_- = [L(s, k) - 1]P^{LF}(s, k)/\hat{E}. \tag{34}$$

5.2. Factorization

To resolve this equation the Green function, $L(s, k)$, should first be factorized, that is presented as

$$L(s, k) = L_+(s, k)(L_-(s, k)), \tag{35}$$

where $L_+(s, k)$ ($L_-(s, k)$) is a regular function in the upper (lower) half-plane of the complex-valued variable k . This can be done using an analogue of the Cauchy-type integral for a periodic function. Eatwell and Willis (1982) and Slepyan (1982) showed that any nonnegative, periodic function $L(k)$ (in our case, the period is equal to 4π)

with locally integrable $\ln L(k)$ can be factorized as follows ($\text{Arg } L = 0$):

$$L_{\pm}(s, k) = \exp \left[\frac{1}{4\pi} \int_{-2\pi}^{2\pi} \ln L(s, \xi) \delta_{\pm}(\xi - k) d\xi \right],$$

$$\delta_{+}(k) = \sum_{\nu=0}^{\infty} e^{-ik\nu/2} = (1 - e^{-ik/2})^{-1} \quad (\Im k \geq 0),$$

$$\delta_{-}(k) = \sum_{\nu=-\infty}^{-1} e^{-ik\nu/2} = e^{ik/2}(1 - e^{ik/2})^{-1} \quad (\Im k \leq 0). \tag{36}$$

In these terms, the governing equation (34) can be presented as

$$L_{+}(s, k)Q_{+} + \frac{Q_{-}}{L_{-}(s, k)} = [L_{+}(s, k) - 1/L_{-}(s, k)]P^{\text{LF}}(s, k)/\hat{E}, \tag{37}$$

where $\Im k = 0$.

We now take the crack-face load to consist of two self-equilibrated forces as in Fig. 2

$$P_2(t, -1, 0)I_2 \quad \text{and} \quad P_5(t, 0, -1)I_5. \tag{38}$$

Then, in accordance with Eq. (29),

$$P^{\text{LF}}(s, k) = P^{\text{L}}(s)e^{-ik/2} [P_2^{\text{LF}}(s, k, 0) = P^{\text{L}}(s)e^{-ik}, P_5^{\text{LF}}(s, k, 0) = 0]. \tag{39}$$

Next, we have to consider the right-hand side of Eq. (37) to separate the terms which can be marked by the subscript ‘+’ and ‘-’. Eq. (37) can be presented as follows:

$$L_{+}(s, k)Q_{+}(s, k) + \frac{Q_{-}(s, k)}{L_{-}(s, k)} = C_{+}(s, k) + C_{-}(s, k) - \frac{1}{L_{-}(s, k)} \frac{P^{\text{L}}(s)}{\hat{E}} e^{-ik/2}, \tag{40}$$

where the last term and C_{-} correspond to functions with the support $m = -1/2, -1, \dots$, while the support of C_{+} is $m = 0, 1/2, 1, \dots$. The sum is

$$C_{+} + C_{-} = C = \frac{P^{\text{L}}(s)}{\hat{E}} L_{+}(s, k)e^{-ik/2}. \tag{41}$$

5.3. Division of the right-hand side

Note that the function L_{+} can be presented as a series

$$L_{+}(s, k) = \sum_{\nu=0}^{\infty} l_{\nu}(s)e^{ik\nu/2} \tag{42}$$

and hence

$$L_{+}(s, k)e^{-ik/2} = l_0(s)e^{-ik/2} + \sum_{\nu=1}^{\infty} l_{\nu}(s) \exp[ik(\nu - 1)/2]. \tag{43}$$

Thus,

$$C_+(s, k) = \frac{P^L(s)}{\hat{E}} \sum_{v=1}^{\infty} l_v(s) \exp[ik(v-1)/2] = \frac{P^L(s)}{\hat{E}} [L_+(s, k) - l_0(s)] e^{-ik/2},$$

$$C_-(s, k) = \frac{P^L(s)}{\hat{E}} l_0(s) e^{-ik/2}. \tag{44}$$

In turn, as follows from Eq. (36)

$$l_0(s) = \exp \left[\frac{1}{4\pi} \int_{-2\pi}^{2\pi} \ln L(s, k) dk \right]. \tag{45}$$

5.4. Solution of the auxiliary problem

Now, if the elongation of the bonds on the crack continuation is to be found, the solution is

$$Q_+(s, k) = \frac{P^L(s)}{\hat{E}} \left[1 - \frac{l_0(s)}{L_+(s, k)} \right] e^{-ik/2}. \tag{46}$$

To find solutions for some bonds in a vicinity of the crack front we rewrite expression (36) for $1/L_+(s, k)$ in the following form ($\Im k > 0$):

$$1/L_+(s, k) = \exp \left[- \sum_{v=0}^{\infty} a_v(s) e^{ikv/2} \right]$$

$$= \frac{1}{l_0} \exp \left[- \sum_{v=1}^{\infty} a_v(s) e^{ikv/2} \right],$$

$$a_v(s) = \frac{1}{4\pi} \int_{-2\pi}^{2\pi} \ln L(s, \zeta) e^{-i\zeta v/2} d\zeta. \tag{47}$$

Thus,

$$Q_+(s, k) = \frac{P^L(s)}{\hat{E}} \left\{ 1 - \exp \left[- \sum_{v=1}^{\infty} a_v(s) e^{ikv/2} \right] \right\} e^{-ik/2}$$

$$= \frac{P^L(s)}{\hat{E}} [a_1(s) + (a_2(s) - a_1^2(s)/2) e^{ik/2}$$

$$+ (a_3(s) - a_1 a_2 + a_1^3(s)/6) e^{ik} + \dots] \tag{48}$$

and the elongations of the crack-path bonds are represented by the coefficients of this exponential series

$$Q_1^L(s) = \frac{P^L(s)}{\hat{E}} a_1(s),$$

$$Q_2^L(s) = \frac{P^L(s)}{\hat{E}} [a_2(s) - a_1^2(s)/2],$$

$$\begin{aligned}
 Q_3^L(s) &= \frac{P^L(s)}{\hat{E}} [a_3(s) - a_1 a_2 + a_1^3(s)/6], \\
 Q_4^L(s) &= \frac{P^L(s)}{\hat{E}} [a_4(s) - a_1(s)a_3(s) - a_2^2(s)/2 + a_2(s)a_1^2(s)/2 - a_1^4(s)/24], \\
 Q_5^L(s) &= \frac{P^L(s)}{\hat{E}} [a_5(s) - a_1(s)a_4(s) - a_3(s)a_2(s) \\
 &\quad + a_3(s)a_1^2(s)/2 + a_1(s)a_2^2(s)/2 - a_2(s)a_1^3(s)/6 + a_1^5(s)/120], \\
 Q_6^L(s) &= \frac{P^L(s)}{\hat{E}} [a_6(s) - a_1(s)a_5(s) - a_4(s)a_2(s) \\
 &\quad + a_4(s)a_1^2(s)/2 - a_3^2(s)/2 + a_3(s)a_1(s)a_2(s) \\
 &\quad - a_3(s)a_1^3(s)/6 + a_2^3(s)/6 - a_2^2(s)a_1^2(s)/4 \\
 &\quad + a_2(s)a_1^4(s)/24 - a_1^6(s)/720] \tag{49}
 \end{aligned}$$

and so on.

6. Solutions for statics

6.1. The auxiliary problem

For the static problem $s = 0$ and Eq. (31) for L yields

$$\begin{aligned}
 L(0, k) &= \frac{A\sqrt{16 \cos^2 k/2 - 8 \cos^4 k/2 - 5 + A}}{\sqrt{22} \sin k/2 [1 + (3 + 4 \cos k/2 - A) \sin^2 k/4]}, \\
 A &= \sqrt{9 + 16 \sin^2 k/2} > 0. \tag{50}
 \end{aligned}$$

From this the coefficients $a_v = a_v(0)$ (47) can be expressed as

$$\begin{aligned}
 a_v &= \frac{1}{2^v} [1 + (-1)^v] + \frac{1}{4\pi} \int_0^{2\pi} \ln[L^0(k)]^2 \cos(kv/2) dk, \\
 L^0(k) &= \frac{A\sqrt{16 \cos^2 k/2 - 8 \cos^4 k/2 - 5 + A}}{\sqrt{2} [1 + (3 + 4 \cos k/2 - A) \sin^2 k/4]}. \tag{51}
 \end{aligned}$$

Note that $\ln[L^0(k)]^2$ is a regular continuous function suitable for numerical integration. In fact, $L^0(k)$ is a positive function; we write here $1/2 \ln[L^0(k)]^2$ to ensure against possible error in the determination of the sign of the square root in the numerator (it changes sign simultaneously with the denominator). The integration results are as follows:

v	1	2	3	4	5	6
a_v	1/4	0.40204668	0.02083333	0.23872244	0.003125000	0.16487307

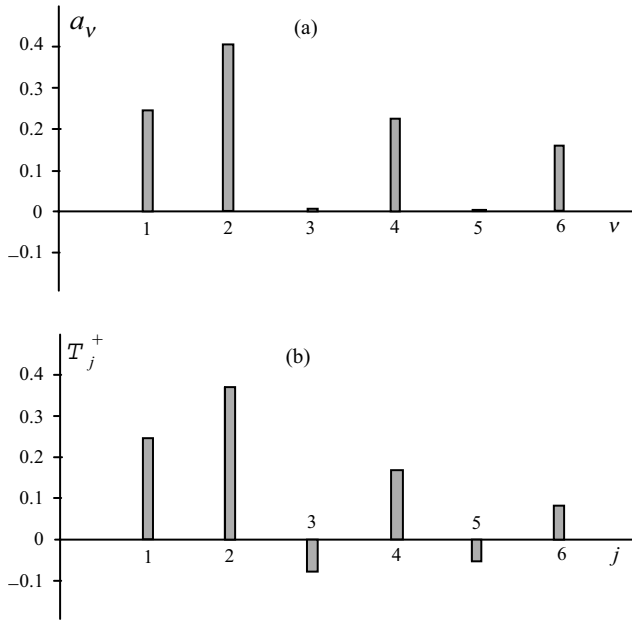


Fig. 3. Static distribution of the tensile forces in the auxiliary problem: (a) the coefficients a_v , (b) the normalized tensile forces T_j^+ .

(Probably, a_v for odd v are rational numbers: $a_1 = 1/4$, $a_3 = 1/48$, $a_5 = 1/320, \dots$) Now the normalized tensile forces, $T_j^+ = T_j^+(\infty) = T_j(\infty)/T_0(0)$, can be found to be

j	1	2	3	4	5	6
T_j^+	1/4	0.37079668	-0.077074171	0.16509454	-0.045114208	0.085767743

The distributions of a_v and T_j^+ are shown in Fig. 3.

The solution obtained here allows us to determine the distribution of the tensile forces ahead of the crack.

6.2. Mode I

Consider a lattice with a semi-infinite crack under mode I deformation caused by remote external forces. In this case, due to symmetry of the lattice, if the first bond, B_0 , disappears, then the tensile force distribution remains the same as in the initial state, but with a one-bond translation, that is, it remains the same relative to the bond at the crack front. This is a distinctive feature of mode I fracture in the triangular-cell lattice. Using superposition with the solution obtained in the previous section, we can write down a recurrence relation for the distribution:

$$T_j + T_j^+ T_0 = T_{j-1}, \quad j = 1, 2, \dots \tag{52}$$

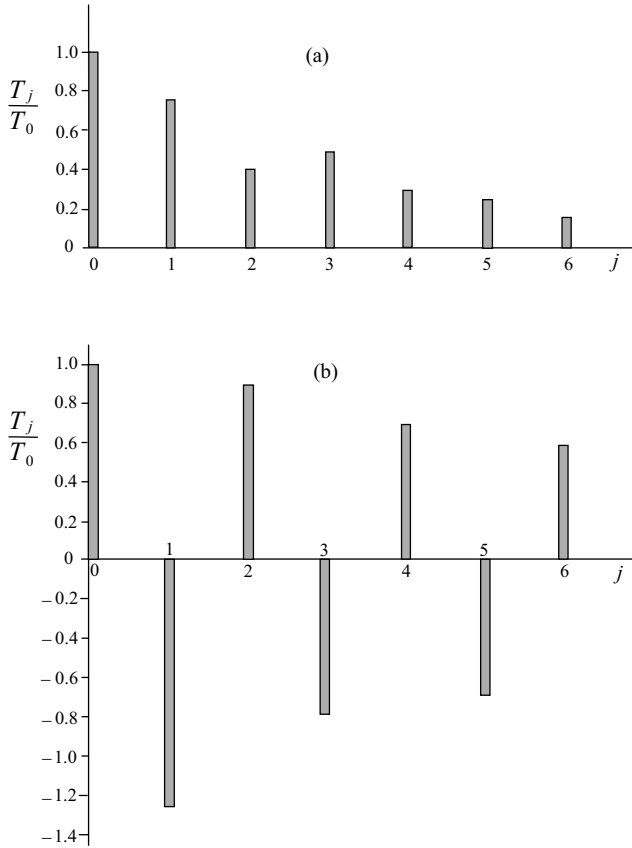


Fig. 4. Static distribution of the tensile forces: (a) mode I, (b) mode II.

Thus, the distribution is

j	1	2	3	4	5	6
T_j/T_0	3/4	0.37920332	0.45627749	0.29118295	0.24606874	0.16030100

So, in mode I, the tensile forces non-monotonically decrease with the distance from the crack-front bond, and what is most important, the force reaches maximum at the first bond (Fig. 4(a)).

6.3. Mode II

In contrast, in the case of mode II, when the first bond, B_0 , disappears, the tensile force distribution in addition to the translation changes sign. The relation is now

$$T_j + T_j^+ T_0 = -T_{j-1}, \quad j = 1, 2, \dots \tag{53}$$

and this leads to the ‘paradoxical’ distribution where the second bond is deformed more than the first:

j	1	2	3	4	5	6
T_j/T_0	-5/4	0.87920332	-0.80212915	0.63703461	-0.68214882	0.59638107

The distribution is shown in Fig. 4(b). We thus face an anomalous distribution where the second bond tensile force, T_1 , is greater than the crack-front one, T_0 . This suggests an irregular behavior of mode II crack. Indeed, if the critical compressive and tensile forces satisfy the inequalities

$$\frac{4}{5} < T_{\text{compressive}}^*/T_{\text{tensile}}^* < \frac{5}{4} \tag{54}$$

then the second bond must break before the first one. Otherwise, such irregular mode of fracture will, at least, alternate with the regular one during slow crack growth. Indeed, in one step of the crack growth, the distribution remains the same (relative to the crack front) but compression is replaced by extension and vice versa. So, if in a crack position the crack-front bond is broken before the second one, then after this the crack-front bond appears to be stronger than the second one and the latter must break previously. No wonder that this irregularity results in an irregular behavior of the crack in dynamics as well.

7. Numerical simulations of crack propagation in a lattice strip

Transient problems are examined numerically using a finite lattice strip. In the auxiliary problem, as well as in a modified auxiliary problem considered below, the field induced by the local self-equilibrated load decreases fast with the distance. This allows us to use a finite lattice of moderate sizes, and the dynamic behavior of several bonds on the crack line appear to be close to that for the infinite lattice—with good accuracy. In contrast, for the crack propagation problems it was important that the strip width is finite. Along with this, the qualitative results appear to be strip-width-independent. We keep here the weak-bond fracture formulation allowing only the bonds between the layers $n = 0$ and 1 to be broken when the elongation reaches the critical value.

7.1. The auxiliary transient problem

A problem similar to that formulated in Sections 3 and 5.4 for the infinite lattice was then considered for a lattice strip with fixed boundaries. The lattice strip with a crack was assumed to be suddenly loaded by a couple of self-equilibrated unit forces shown in Fig. 2. The dynamics of the first five bonds on the crack continuation was examined. The strip sizes were taken so large (up to $|m| \leq 100, |n| \leq 50$) that the results are insensitive to the reflection from the boundary with accuracy up to the sixth significant digit. The same requirement was satisfied for the modified auxiliary problem (see below). This was checked by lattice size variation and by comparison of the results for a large time with those found analytically for the infinite lattice in statics.

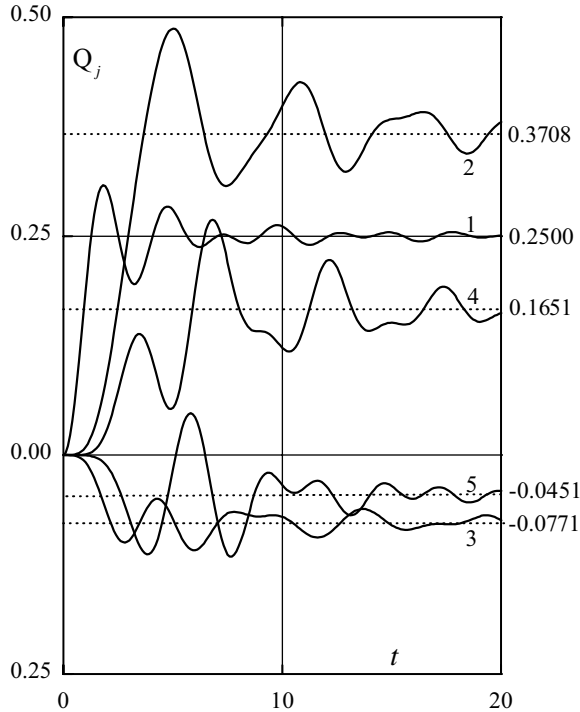


Fig. 5. Elastic bond elongation in the transient auxiliary problem. The dotted lines correspond to the static values found analytically.

The goal of the numerical examination of the auxiliary problems was (a) to describe how the irregular distribution of the tensile forces found analytically in statics is established, (b) to determine the influence of viscosity on this process and (c) to obtain the separation between the domains of the static amplitude response (SAR) and the dynamic overshoot response (DOR) on the plane of the creep and relaxation times—as was done for the mode III square-cell lattice in Slepyan (2000).

The transient problem results for the elastic lattice are shown in Fig. 5 where the dotted lines correspond to the static values found analytically (see Section 6.1 and Fig. 3(b)). Recall that the units are used such that tensile forces and elongations in the elastic lattice coincide. With the above-mentioned accuracy numerically obtained values of $Q_1(t)$ coincide with the corresponding static values T_1^+ for $t > 30$ (recall that $T_j^+ = T_j^+(\infty)$). The dynamic amplification factor for the first bond is found to be equal to 1.229.

In an initial stage of the process, the second bond elongation is lower than the first, but then it becomes higher. Also the dynamic factor for the second bond is somewhat greater; it is equal to 1.330. It is of interest that for even bonds the amplitudes of the oscillations of Q_j relative to the static values are higher and the frequencies are considerably lower than those for the odd bonds. The second bond

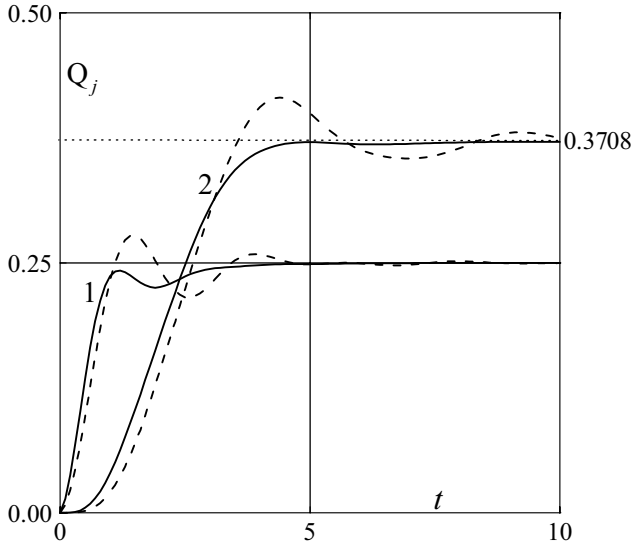


Fig. 6. The first two viscoelastic bond elongation in the transient auxiliary problem. Solid curves: $\alpha = 1.0, \beta = 0.25$; dashed curves: $\alpha = 1.0, \beta = 0.5$ (1. $j = 1, 2. j = 2$).

elongation approaches the static value with the above-mentioned accuracy when $t > 42$.

An example of the first two bonds elongations for a lattice made of the standard viscoelastic material is presented in Fig. 6. It can be seen that in the case $\alpha = 1, \beta = 0.25$ there is no overshoot; this pair falls into the SAR domain, while the pair $\alpha = 1, \beta = 0.5$ belongs to the DOR domain.

Mode II tensile force distribution (see Section 6.3 and Fig. 4(b)) suggests irregular crack growth, namely, if, under high viscosity, the crack grows slowly, then the second bond can break before the first one (recall that the bonds are numbered beginning from the crack front). The first bond breaks soon thereafter. Then the time-interval till the next break is as large as the averaged (macrolevel) crack speed is low. Thus, the crack advance appears to be a repeated two-step process as ‘the second bond break—a short time-interval—the first bond break—a long time-interval’, and so on.

To analyze the dynamic factor manifestation in such a process the formulation of the auxiliary problem related to mode II is modified. Let us suggest that a couple of the bonds, the crack-front bond and the next one, break simultaneously. To model the transient process arising as a result of such double break we have to apply two pairs of forces: P_0 and P_1 as shown in Fig. 7(a). The former reflects the front bond break (numbered 0) as in the above auxiliary problem, while the latter (numbered 1) reflects the next bond break. In accordance with the initial tensile forces in mode II we take $P_0 = 1, P_1 = 1.25$. First, we consider an elastic lattice strip. The dynamic elongation of the first four intact bonds is shown in Fig. 7(b). It can be seen that elongations in alternate bonds have opposite signs. Contrary to the one-break auxiliary problem, the

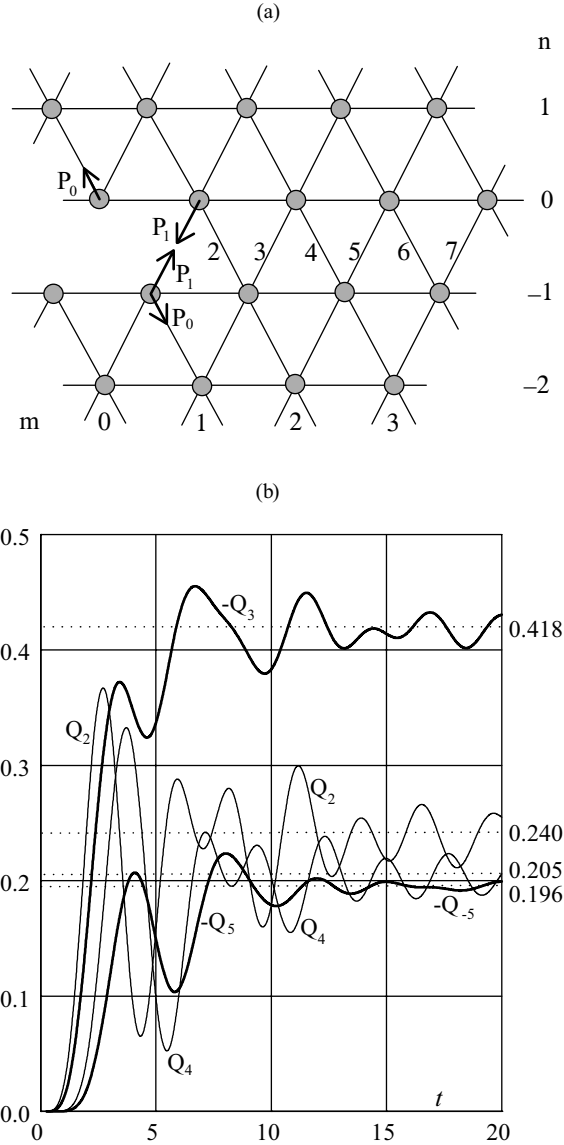


Fig. 7. The modified auxiliary problem: (a) external forces, (b) elastic bond transient elongation. The dashed lines correspond to the static values, $Q_2(\infty) \approx 0.240$, $Q_3(\infty) \approx -0.418$, $Q_4(\infty) \approx 0.205$, $Q_5(\infty) \approx -0.196$.

dynamic factor for the first intact bond, $j = 2$, equal to 1.517 is greater than that for the second which is equal to 1.069.

An example of the dynamic elongation of the first two intact viscoelastic bonds is shown in Fig. 8. In the case $\alpha=0.5$, $\beta=0.4$, an overshoot is revealed for both elongations

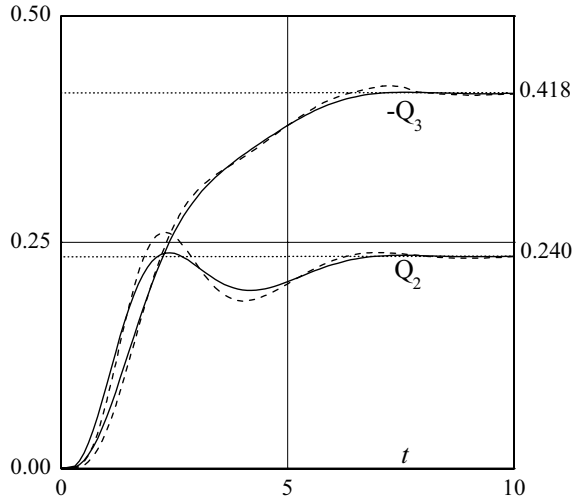


Fig. 8. Viscoelastic bond elongation in the modified transient auxiliary problem. Solid curves: $\alpha=0.5, \beta=0.2$; dashed curves: $\alpha=0.5, \beta=0.4$.

Q_2 and Q_3 . So, this pair lies in the DOR domain. In the case $\alpha=0.5, \beta=0.2$, an overshoot is observed only for Q_2 ; however, the absolute value of Q_3 is significantly greater than Q_2 . Taking this into account we define the domain, whether the couple of the viscosity times belongs to the DOR or to the SAR domain, based on the behavior of the highest elongation, Q_3 . The latter case thus belongs to the SAR domain.

The SAR/DOR interfaces corresponding to the auxiliary problem (curve I) and the modified, double-break auxiliary problem (curve II) are shown in Fig. 9. The SAR domain lies beneath the corresponding curve, while the DOR domain lies above it.

7.2. Mode I crack propagation

A lattice strip was considered with the sizes up to $|m| \leq 1100, |n| \leq 50$, while the main numerical simulations were performed for the strip $|m| \leq 400, |n| \leq 10$. Two static states were introduced. In the initial state (denoted as S_1) the two families of slope bonds were uniformly lengthened by the given elongation Q^0 , while the horizontal bonds remained at rest. After this the strip boundaries were fixed. At moment $t=0$, a ‘semi-infinite’ crack was introduced, that is the bonds $B_4(j,0), j \leq -1$ and $B_5(j,0), j \leq -2$ were removed as in Fig. 1(a). Under the influence of viscosity, the dynamic process caused by this action settled down and a new static state was approached. We denote it as S_2 . In this latter state, the distribution of the elongations of the intact bonds on the crack line, $j=0, 1, \dots$, is under our attention. The maximum of the absolute value of these elongations is denoted by Q_*^0 . Note that in mode I this maximum appears at the first intact bond, $j=0$. Further, the critical elongation Q_c is introduced which determines the elongation resulting in the bond destruction. We

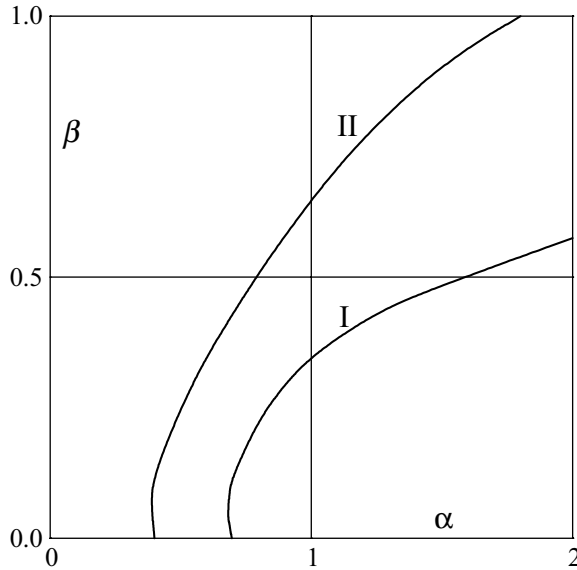


Fig. 9. SAR/DOR domains separation. Curves I and II correspond to modes I and II, respectively. The SAR domain lies beneath the corresponding curve, while the DOR domain lies above it.

do not consider the trivial case $Q^0 > Q_*^0$ and hence to get the crack propagation we have to assume that $Q^0 < Q_c < Q_*^0$. The limiting elongation Q_c is fixed; without loss of generality we take $Q_c = 1$.

Under the same Q^0 the value of Q_*^0 appeared to be proportional to the square root of the strip width, which is in agreement with the conclusion following from energy considerations. Simulations were performed for the strips with $|n| \leq N$, $N = 10, 20$ and 50 . It was found that peculiarities of crack propagation are controlled by the values of Q^0 and Q_*^0 . If these values are fixed, no qualitative influence of the strip width on the crack propagation was observed.

Some results related to mode I crack propagation are shown in Figs. 10–16. We took $N = 10$. This resulted in $Q_*^0 = 2.405Q^0$. The latter, Q^0 , was varying in the range $1/2.405 \approx 0.416 < Q^0 < 1$ (for the lower bound Q_*^0 is equal to the limiting elongation). In these figures, the dotted lines correspond to the long Rayleigh wave speed, $c_R = \frac{1}{2}\sqrt{3 - \sqrt{3}} \approx 0.563$, while the dash-dotted lines correspond to the long longitudinal wave speed, $c_1 = \sqrt{9/8} \approx 1.061$.

Let us denote by $t(j)$ the j th bond break time counted from the moment when the crack started to propagate. Ray-like curves in Figs. 10 and 12–14 are dependences obtained by successive joining of the corresponding discrete values. In Fig. 10, these dependences are shown for various initial elongations Q^0 for the elastic lattice strip. The hollow (solid) circles are related to the even (odd) bonds (in Figs. 10(a),(b) each bond is marked by a circle, while in Figs. 10(d)–(f) the curves $t(j)$ connecting the corresponding bonds are marked). As can be seen in Figs. 10 and 12–14, a transient stage

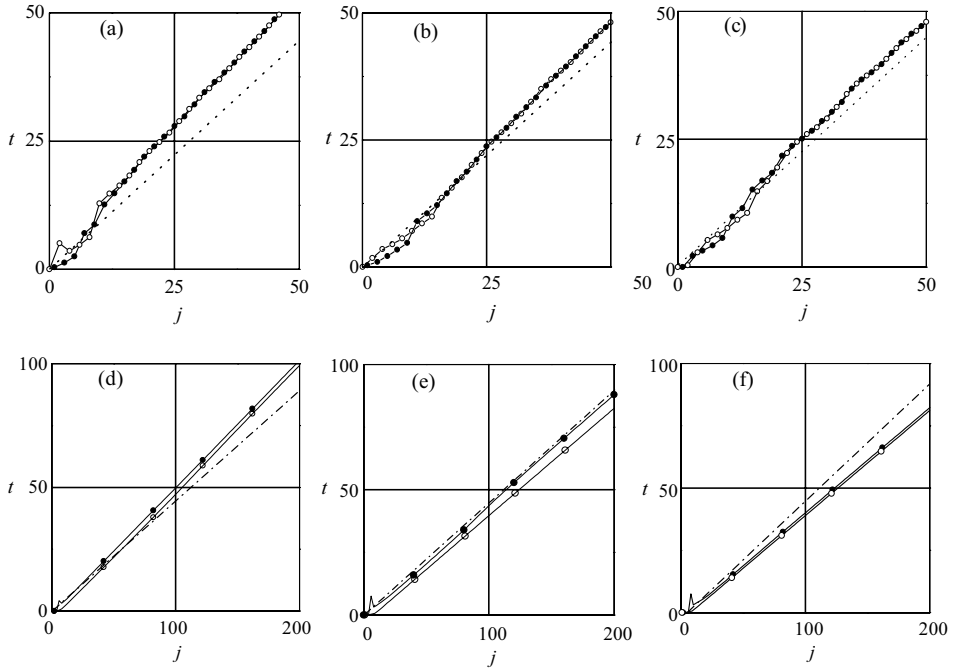


Fig. 10. Bond-break time versus the bond number for mode I fracture of the elastic strip. The odd bonds are marked by hollow circles and the even bonds are marked by solid circles. The dotted lines correspond to the long Rayleigh wave speed, while the dash-dotted lines correspond to the long longitudinal wave speed: (a) $Q^0 = 0.416667$ ($Q_*^0 = 1.00189$), (b) $Q^0 = 0.5$ ($Q_*^0 = 1.20226$), (c) $Q^0 = 0.6$ ($Q_*^0 = 1.44272$), (d) $Q^0 = 0.9$ ($Q_*^0 = 2.16408$), (e) $Q^0 = 0.935$ ($Q_*^0 = 2.24824$), (f) $Q^0 = 0.95$ ($Q_*^0 = 2.28430$).

of the crack propagation is followed by a quasi-steady regime which is characterized by almost straight-line parts of the dependences.

In general, the bonds break in order; however, we met a situation where it was not so. It appeared that a difference can exist between the speeds of fracture of the odd and even bonds. In such a case, there exists a *binary* crack consisting of two branches expanding along the same line. This phenomenon suggests the introduction of two speeds, one, v_1 , for the odd-bond branch and another, v_2 , for the even-bond branch. Although this phenomenon is most pronounced for mode II crack propagation, it can manifest itself in mode I as well. In the latter case, this can happen within a rather narrow range of the initial state parameters. Three cases are revealed in the analysis of the crack propagation:

- (i) The speeds are equal, $v_1 = v_2$, and there is no time delay in the successive breaking of the odd and even bonds. In this regular case, a single crack speed exists, $v = v_1 = v_2$ and the conventional definition of the crack is valid.
- (ii) The speeds are equal, $v_1 = v_2$; however, a small but visible distance between the fronts of the two crack branches exists. This is a *one-speed binary crack*. From

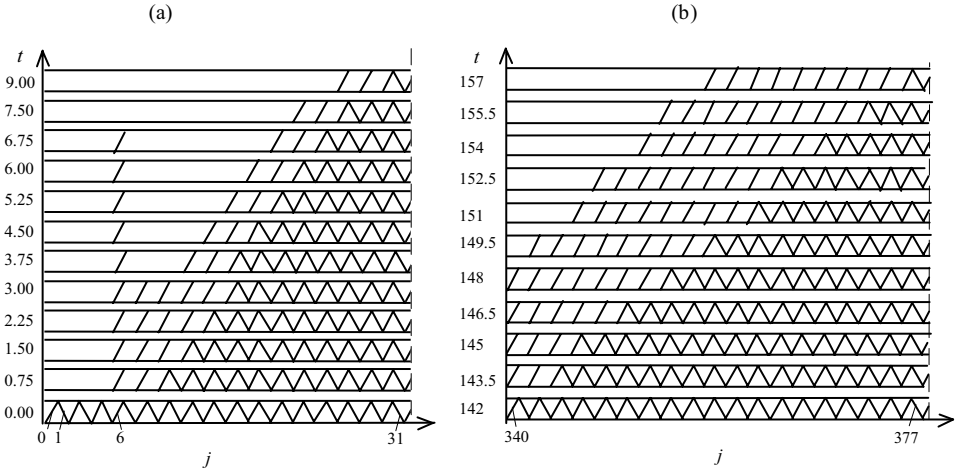


Fig. 11. Mode I binary crack for $Q^0 = 0.935$. Intact bonds are shown: (a) Transient regime, (b) Quasi-steady-state crack propagation.

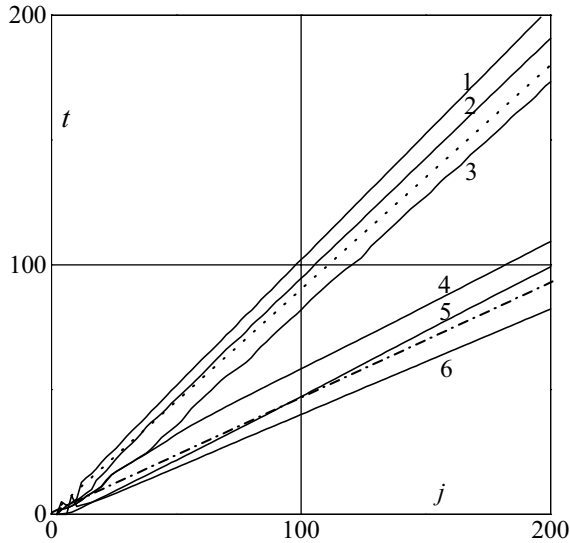


Fig. 12. The gap in the elastic mode I crack speed. 1. $Q^0 = 0.4167$, 2. $Q^0 = 0.5$, 3. $Q^0 = 0.765616$, 4. $Q^0 = 0.765617$, 5. $Q^0 = 0.8$, 6. $Q^0 = 0.95$. The dotted lines correspond to the long Rayleigh wave speed, while the dash-dotted lines correspond to the long longitudinal wave speed.

the macrolevel point of view it is regular crack propagation with a fixed ‘fracture process zone’.

(iii) The speeds are not equal, $v_1 \neq v_2$. This is a real *two-speed binary crack*.

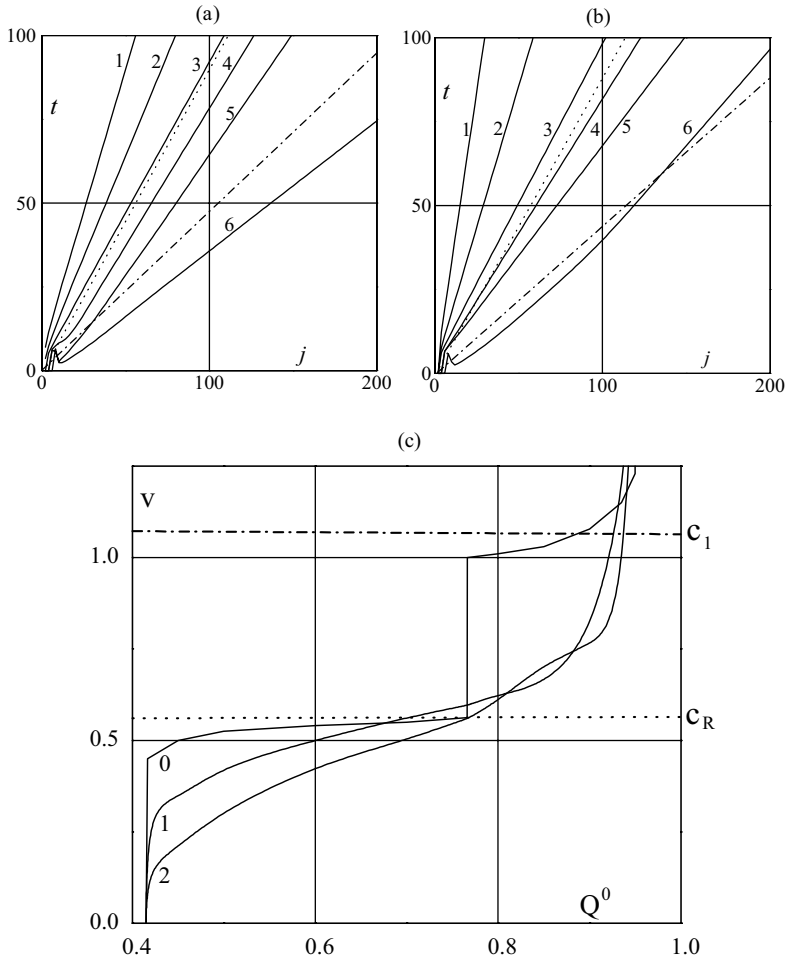


Fig. 13. Mode I crack propagation in the viscoelastic lattice strip with $\beta=0$. Dependences $j(t)$ for (a) $\alpha=1$, (b) $\alpha=2$. 1. $Q^0=0.4167$, 2. $Q^0=0.5$, 3. $Q^0=0.7$, 4. $Q^0=0.8$, 5. $Q^0=0.9$, 6. $Q^0=0.95$. (c) Crack speed versus Q^0 ; the values of α ($\alpha=0, 1, 2$) are shown.

These three cases are presented in Fig. 10. The first case (i) is realized in the interval $0.416 < Q^0 < 0.766$ ($1 < Q_*^0 < 1.841$). In this interval the crack speed varies increasing together with Q^0 up to a value somewhat higher than c_R . Examples are presented in Fig. 10(a)–(c).

The next case, (ii) corresponds to a relatively strong initial elongation, $Q^0 > 0.766$ ($Q_*^0 > 1.841$). When Q^0 exceeds this value, the crack speed jumps to a close vicinity of the long longitudinal wave speed, c_1 (as reflected in Fig. 12). The crack speed remains approximately equal to c_1 in the elongation range $0.766 < Q^0 < 0.925$ and then increases as Q^0 increases, Figs. 10(d)–(f). Note that the ‘experimental’ fact that the interval $c_R < v < c_1$ is forbidden is in agreement with the theoretical results obtained

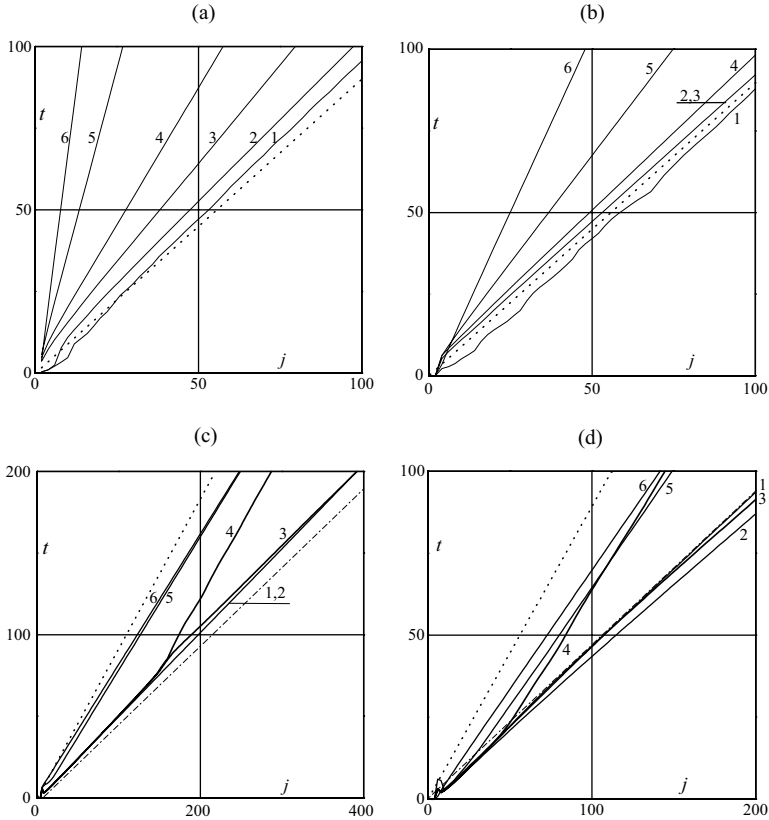


Fig. 14. Mode I crack propagation in the viscoelastic lattice strip with the speed discontinuities: (a) $Q^0 = 0.5$; 1. $\alpha = 0$, 2. $\alpha = 0.25$, 3. $\alpha = 1$, 4. $\alpha = 2$, 5. $\alpha = 5$, 6. $\alpha = 10$. (b) $Q^0 = 0.7$; 1. $\alpha = 0$, 2. $\alpha = 0.25$, 3. $\alpha = 1$, 4. $\alpha = 2$, 5. $\alpha = 5$, 6. $\alpha = 10$; (c) $Q^0 = 0.8$; 1. $\alpha = 0$, 2. $\alpha = 0.1$, 3. $\alpha = 0.141$, 4. $\alpha = 0.142$, 5. $\alpha = 1$, 6. $\alpha = 2$; (d) $Q^0 = 0.9$; 1. $\alpha = 0$, 2. $\alpha = 0.25$, 3. $\alpha = 0.355$, 4. $\alpha = 0.356$, 5. $\alpha = 1$, 6. $\alpha = 2$. The dotted lines correspond to the long Rayleigh wave speed, while the dash-dotted lines correspond to the long longitudinal wave speed.

for steady-state crack propagation in the infinite triangular lattice, see Slepyan (2001).

Case (iii) is realized if Q^0 falls within a narrow range, $0.93 < Q^0 < 0.94$ (see Fig. 10(e)). The speeds are $v_1 \approx 1.06$, $v_2 \approx 1.09$. Note that this case is exceptional for mode I crack propagation, while it is more common for mode II (see below).

In a different form, the dependences of Fig. 10(e) are shown in Fig. 11, where the crack-path layer with broken bonds removed is represented for a set of time-moments. In the initial crack propagation stage, the space delay between fracture fronts corresponding to the odd and even bonds is equal to two-bond distance (Fig. 11(a), $t \approx 9.00$), while it continuously increases in the quasi-steady-state stage as shown in Fig. 11(b). For example, the space delay increases to nine-bond distance at $t \approx 155$. The main effect found for mode I crack propagation is a gap in the crack speeds between

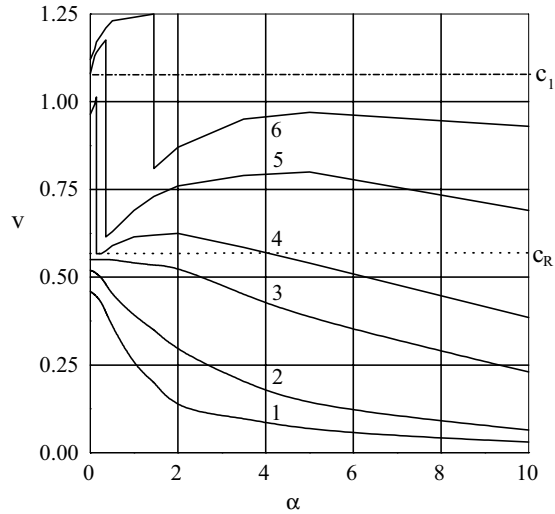


Fig. 15. Mode I crack speed versus creep time, α ($\beta = 0$). 1. $Q^0 = 0.4167$, 2. $Q^0 = 0.5$, 3. $Q^0 = 0.7$, 4. $Q^0 = 0.8$, 5. $Q^0 = 0.9$, 6. $Q^0 = 0.95$.

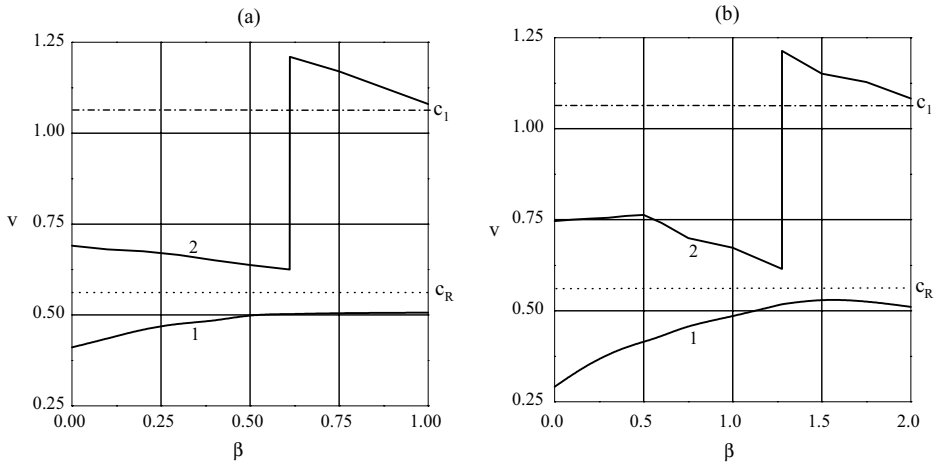


Fig. 16. Mode I crack speed versus relaxation time, β : (a) $\alpha = 1$; (b) $\alpha = 2$. 1: $Q^0 = 0.5$, 2: $Q^0 = 0.9$.

the Rayleigh and longitudinal long wave speeds. As can be seen in Fig. 12, the crack speed jumps over this gap when Q^0 increases from the value 0.765616 to 0.765617.

We now turn to peculiarities of crack propagation in a viscoelastic lattice strip. In Figs. 13(a), (b) dependences $v(j)$ are depicted for two values of the creep time, $\alpha = 1$ and 2 (with zero relaxation time) and for a set of Q^0 . It can be seen how v decreases with an increase of α . Contrary to the elastic case, the crack speeds can fall within the forbidden interval (c_R, c_1). Dependences $v(Q^0)$ are shown in Fig. 13(c) for $\alpha = 0, 1$

and 2. It can be seen that there exists a jump discontinuity in the elastic case, while the dependences are continuous for $\alpha = 1$ and 2.

Note that curve 6 ($Q^0 = 0.935$) in Fig. 13(b) (contrary to other dependences) has a change in slope at $t \approx 42$, $j = 95$. Before this the crack speed $v \approx c_1$, while $v \approx 0.762$ after this. Further analysis shows that this fact is related to the jump-like character of the dependence $v(\alpha)$ in the case of a relatively strong initial elongation.

A comparison of the dependences $t(j)$ built for a set of α is presented in Figs. 14(a), (b) for low initial elongations and in Figs. 14(c), (d) for high elongations. In the latter, discontinuities can be seen in the dependences $v(\alpha)$. It was found that such discontinuities exist for those values of Q^0 which, in the elastic case, result in sonic–supersonic crack propagation (i.e. if $Q^0 \geq 0.7656$). Dependences of the crack speed versus α are shown for several Q^0 in Fig. 15.

It was found that the critical value of $\alpha = \alpha^*$ corresponding to the jump in the crack speed increases with Q^0 . Some values of α^* are as follows:

$$\begin{aligned} \alpha^* = 0 \quad (Q^0 = 0.765616), \quad \alpha^* = 0.141 \quad (Q^0 = 0.8), \\ \alpha^* = 0.355 \quad (Q^0 = 0.9), \quad \alpha^* = 1.452 \quad (Q^0 = 0.935). \end{aligned} \tag{55}$$

This phenomenon is also manifested in the case of the standard viscoelastic material with $\alpha > \beta > 0$. Crack speed dependences $v(\beta)$ for $\alpha = 1$ and 2 ($Q^0 = 0.5$ and 0.9) are presented in Fig. 16.

7.3. Mode II crack propagation

The main numerical simulations for mode II fracture were performed for the strip $|m| \leq 800$, $|n| \leq 10$. Here, the static state S_1 is obtained by means of the slope bonds lengthening and shortening which alternate with m ; specifically, the right-slope bonds are under compression, while the left-slope bonds are under extension. As in the mode I problem, the horizontal bonds remain unstressed. Here the left-slope bond initial elongation is denoted by Q^0 . So, the right-slope bond initial elongation is $-Q^0$. For $|n| \leq 10$ the elongation of the zero bond, in the mode II S_2 -state, appears to be $Q_*^0 = 2.950Q^0$. The range of Q^0 is thus $1/2.950 \approx 0.339 < Q^0 < 1$.

First of all, we note a phenomenon which, along with the fact that $|Q_1| > Q_0$ in the S_2 -state, can result in irregular crack propagation. It is manifested in the process shown in Fig. 17 as the dynamic transition from the S_2 -state to a new static state, S_3 , which corresponds to the lattice strip with all the odd (compressed) bonds on the crack line removed.

A surprising result can be seen: in the S_3 -state, the intact bond elongations appear to be lower than in the S_2 -state. So, the odd bonds reduce the strength of the lattice. Note, however, that this effect exists when the strip is deformed by a ‘rigid machine’, that is when its boundaries are fixed.

Cases (i) and (ii) considered for mode I exist in mode II as well; however, case (iii) is here the most pronounced. What is more, in mode II the two branches of the binary crack can change places. In some numerical situations, $v_1 < v_2$, while $v_1 > v_2$ in

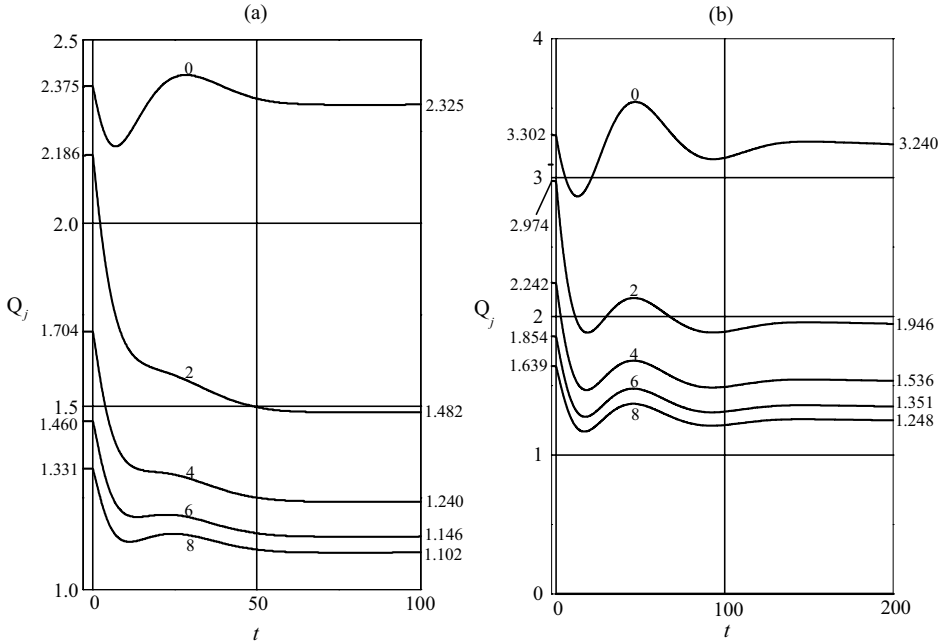


Fig. 17. Transition from \$S_2\$-state to the \$S_3\$-state for mode II: (a) \$|n| \le 10\$, (b) \$|n| \le 20\$. Numbers of the intact bonds are shown.

others. In addition, the quasi-steady-state mode II crack can propagate with a periodic exchange of the speeds of its branches.

The numerical simulation results are presented in Figs. 18–22. As above, the dotted lines correspond to Rayleigh wave speed, \$c_R\$, while the dash-dotted lines—to \$c_1\$. The limiting elongation and contraction are taken to be the same, \$|Q_c| = 1\$.

Dependences \$t(j)\$ for the elastic case are depicted in Figs. 18(a). Here, as in mode I, the hollow circles correspond to the even bonds, while the solid circles correspond to the odd bonds. At a very low elongation, \$Q^0 = 0.34\$ (\$Q_*^0 = 1.002\$)—couple of curves 1—case (ii) is realized: \$v_1 = v_2 \approx 0.397\$, the odd-bond branch propagates ahead, the time delay is approximately 55.15. Recall that the size unit is the bond length, \$a\$, and the speed unit is \$c = a\sqrt{E/M}\$.

With increase in \$Q^0\$ the order of the branches is changed. The initial elongation \$Q^0 = 0.375\$ (\$Q_*^0 \approx 1.105\$)—curves 2—again results in case (ii): \$v_1 = v_2 \approx 0.451\$, but now the even-bond branch propagates ahead. For a somewhat higher initial elongation, \$Q^0 = 0.4\$ (\$Q_*^0 \approx 1.179\$)—curves 3—case (iii) is realized with \$v_1 \approx 0.495\$, \$v_2 \approx 0.791\$. Then, if \$Q^0\$ is varied in a relatively wide interval, from \$Q^0 = 0.4167\$ (\$Q_*^0 \approx 1.230\$)—curves 4—till \$Q^0 = 0.95\$ (\$Q_*^0 \approx 2.80\$)—curves 5—the regular case (i) is realized, where the crack velocity falls into the small vicinity of \$c_1\$ slowly increasing from \$v \approx 0.998\$, curves 4, till \$v \approx 1.15\$, curves 5. At a very high elongation \$Q^0 = 0.99\$ (\$Q_*^0 \approx 2.98\$)—curves 6—case (ii) is returned with \$v_1 = v_2 \approx 1.51\$, the odd-bond branch propagates ahead and the time delay is approximately 9.25.

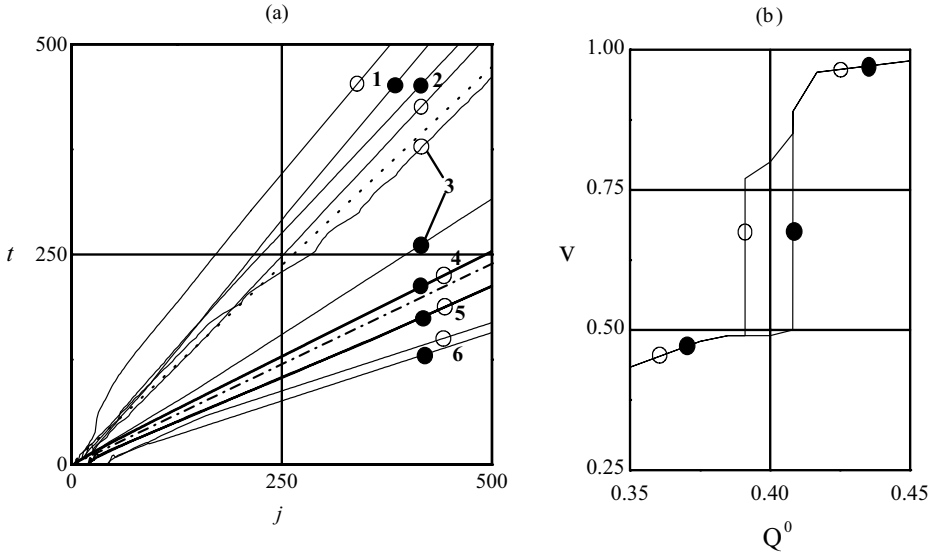


Fig. 18. Mode II binary crack propagation in the elastic lattice strip. The odd bonds are marked by hollow circles and the even bonds are marked by solid circles. The dotted lines correspond to the long Rayleigh wave speed, while the dash-dotted lines correspond to the long longitudinal wave speed: (a) The binary crack fronts versus time. 1. $Q^0 = 0.34$ ($Q_*^0 \approx 1.002$), 2. $Q^0 = 0.375$ ($Q_*^0 \approx 1.105$), 3. $Q^0 = 0.4$ ($Q_*^0 \approx 1.180$), 4. $Q^0 = 0.4167$ ($Q_*^0 \approx 1.230$), 5. $Q^0 = 0.95$ ($Q_*^0 \approx 2.80$), 6. $Q^0 = 0.99$ ($Q_*^0 \approx 2.98$). (b) Discontinuities in the binary crack speeds.

Crack speed as a function of Q^0 in the vicinity of $Q^0 = 0.4$ is presented in Fig. 18(b). Two jump discontinuities, one in v_1 and another in v_2 exist at $Q^0 = 0.391$ and 0.408 , respectively.

Dependences $t(j)$ in the viscoelastic lattice strip are shown in Fig. 19 for an intermediate elongation $Q^0 = 0.7$ ($Q_*^0 \approx 2.07$) and for a set of values of the creep time, α ($\beta = 0$). It can be seen how crack velocities decrease with increase in α from a vicinity of c_1 to the Rayleigh wave speed and below it.

In the case of high initial elongation, $Q^0 = 0.9$ ($Q_*^0 \approx 2.65$), the supersonic regime of crack propagation is realized, Fig. 20. In this figure, the effect of velocity exchange can be observed.

In the case of the elastic lattice, Fig. 20(a), case (i) is revealed. At $\alpha = 0.25$, Fig. 20(b), the quasi-steady-state crack propagation is characterized by a periodic exchange of the crack speeds between the branches. With further increase in α , Figs. 20(c) and (d), such exchange can be realized at an initial unsteady stage, while the quasi-steady-state regime is related to case (iii).

A special regime of case (iii) with zero speed of one of the branches of the binary crack can occur. This looks like the bridging by fibers appearing in fracture of fiber-reinforced composites (Budiansky et al., 1986; Willis, 1993; Meda and Steif, 1994a,b; Movchan and Willis, 1996, 1997a,b, 1998; Nemat-Nasser and Luqun, 2001). In connection with the binary crack phenomenon, the Barenblatt

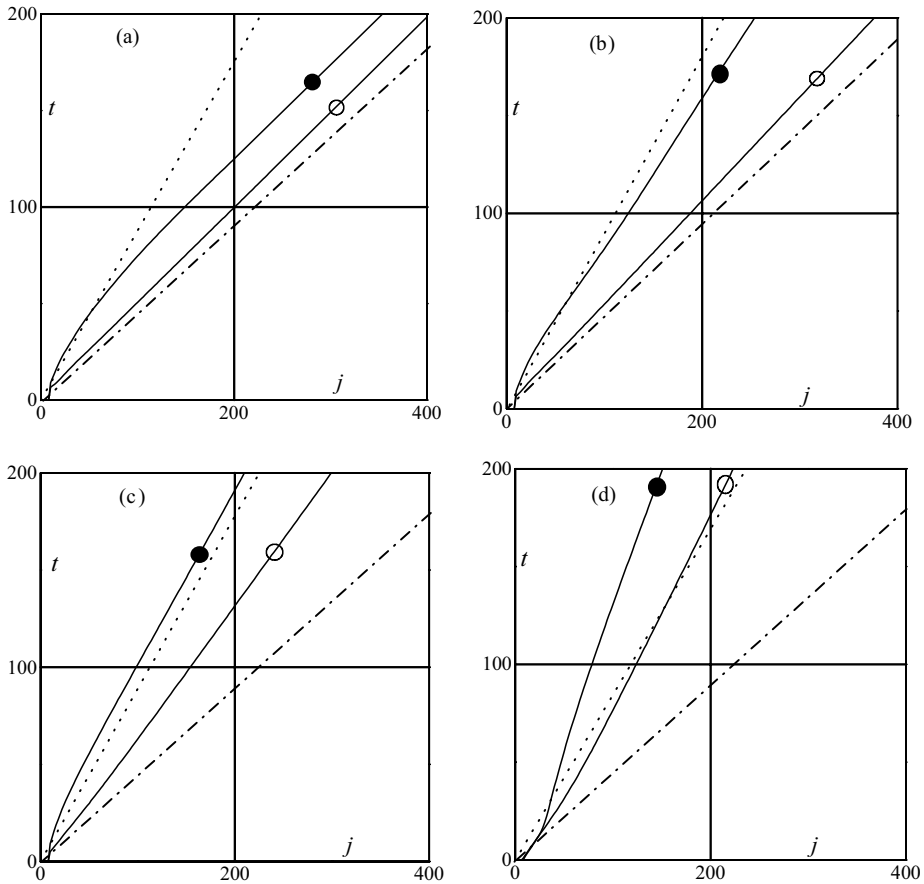


Fig. 19. Mode II binary crack propagation in the viscoelastic lattice strip for $Q^0 = 0.7$ under different values of creep time α ($\beta = 0$): (a) $\alpha = 1$, (b) $\alpha = 2$, (c) $\alpha = 5$, (d) $\alpha = 10$. The odd bonds are marked by hollow circles and the even bonds are marked by solid circles. The dotted lines correspond to the long Rayleigh wave speed, while the dash-dotted lines correspond to the long longitudinal wave speed.

cohesive zones in polymers are worthy of note (Knauss, 1973, 1993; Lauterwasser and Kramer, 1979).

In Figs. 21(a) and (b), the even- and the odd-bond branches are, respectively, shown for various values of Q^0 and $\alpha = 1, \beta = 0$. The calculations show that in this case the crack does not propagate, $v_1 = v_2 = 0$, if $Q^0 \leq 0.351$. The speeds v_1 and v_2 shown in Fig. 21 are

Q^0	0.357	0.417	0.5	0.6	0.7	0.8	0.9	0.95
v_1	0	0	0.495	0.523	1.02	1.21	1.44	1.78
v_2	0.141	0.382	0.515	0.878	1.01	1.12	1.38	1.68

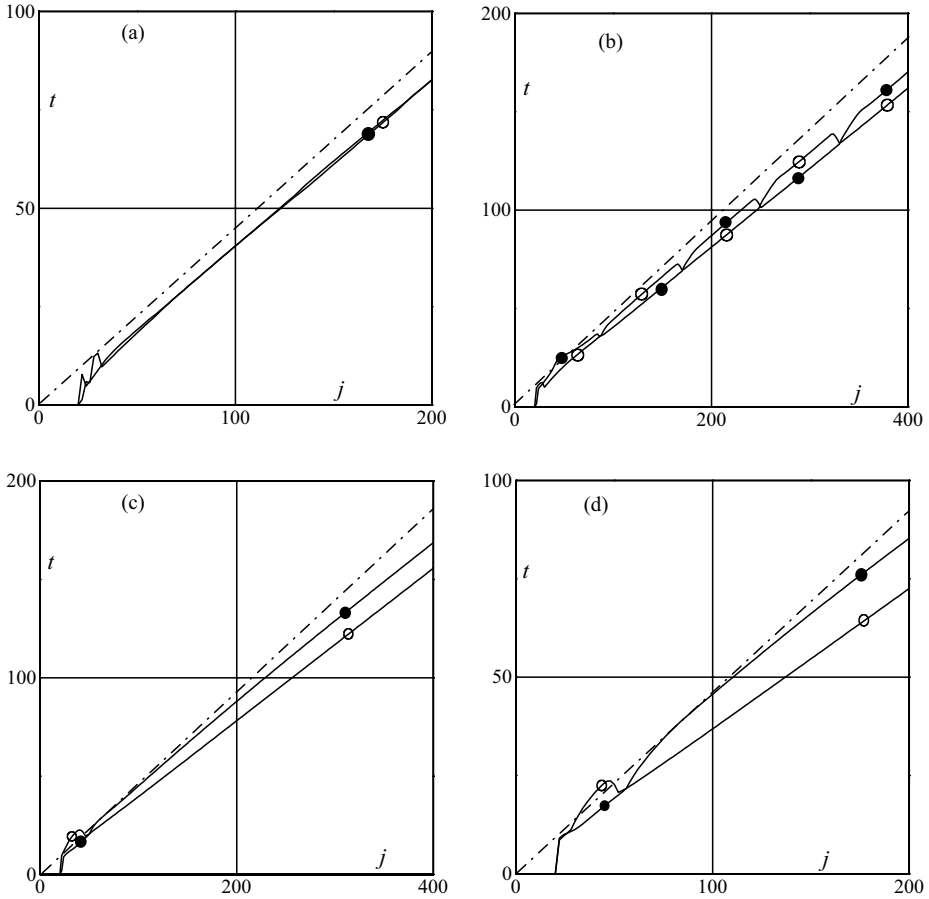


Fig. 20. Mode II binary crack propagation in the viscoelastic lattice strip for $Q^0 = 0.9 (Q_*^0 = 2.65)$ under different values of creep time α ($\beta = 0$): (a) $\alpha = 0$, (b) $\alpha = 0.25$, (c) $\alpha = 0.5$, (d) $\alpha = 1$. The odd bonds are marked by hollow circles and the even bonds are marked by solid circles. The dash-dotted lines correspond to the long longitudinal wave speed.

Speeds v_1 and v_2 have discontinuities in the intervals $0.6 < Q^0 < 0.7$ and $0.5 < Q^0 < 0.6$, respectively. It is of interest that $v_1 < v_2$ before the jump of v_1 ($Q^0 < 0.6$), while $v_1 > v_2$ after the jump ($Q^0 > 0.6$).

Speed jumps and the presence of different crack branches can be realized with variation of the relaxation time as well. An example is represented in Fig. 22 where (a) even and (b) odd branches are shown for $Q^0 = 0.5$, $\alpha = 0$ and various values of β . It can be seen that v_1 being lower than c_R for $\beta \leq 0.75$ jumps to c_1 in the interval $0.75 < \beta < 1$, while $v_2 \approx c_R$ in the interval $0 < \beta < 0.5$ and jumps to a value higher than c_1 in the interval $0.5 < \beta < 0.75$.

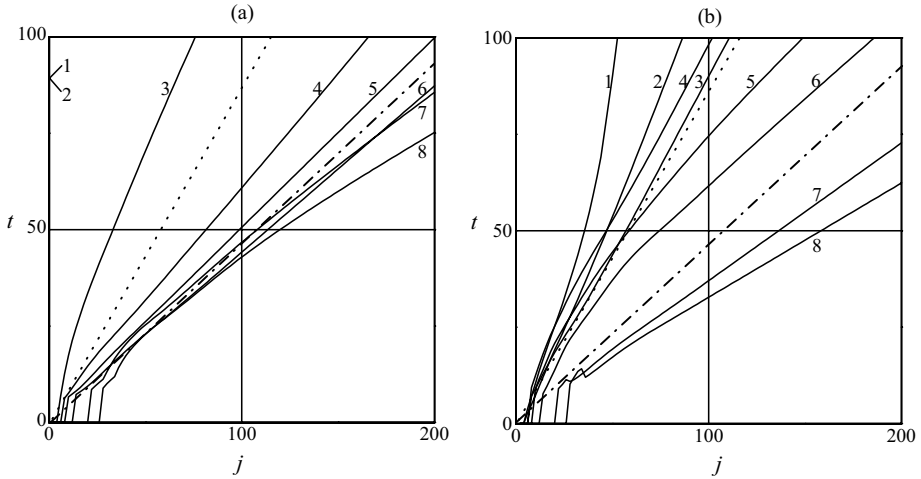


Fig. 21. Mode II binary crack propagation in the viscoelastic lattice strip for $\alpha = 1$, $\beta = 0$: (a) Even-bond branch, (b) Odd-bond branch. 1. $Q^0 = 0.36 (Q_*^0 = 1.062)$, 2. $Q^0 = 0.42 (Q_*^0 = 1.239)$, 3. $Q^0 = 0.5 (Q_*^0 = 1.475)$, 4. $Q^0 = 0.6 (Q_*^0 = 1.770)$, 5. $Q^0 = 0.7 (Q_*^0 = 2.06)$, 6. $Q^0 = 0.80 (Q_*^0 = 2.36)$, 7. $Q^0 = 0.9 (Q_*^0 = 2.65)$, 8. $Q^0 = 0.95 (Q_*^0 = 2.80)$. The dotted lines correspond to the long Rayleigh wave speed, while the dash-dotted lines correspond to the long longitudinal wave speed.

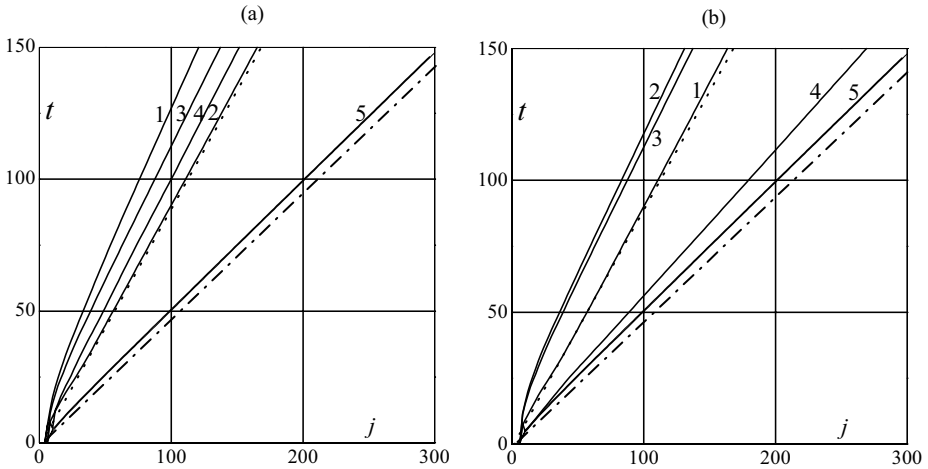


Fig. 22. Mode II binary crack propagation in the viscoelastic lattice strip for $Q^0 = 0.5$, $\alpha = 1$ and various values of β : (a) Even-bond branch, (b) Odd-bond branch. 1. $\beta = 0$, 2. $\beta = 0.25$, 3. $\beta = 0.5$, 4. $\beta = 0.75$, 5. $\beta = 1$. Rayleigh wave speed, while the dash-dotted lines correspond to the long longitudinal wave speed.

8. Conclusion

Elastic and viscoelastic (standard material) quasi-static and dynamic crack growth in the unbounded triangular lattice and in a lattice strip deformed by a ‘rigid machine’

was examined. A crack was assumed to propagate along a given layer of lattice bonds, while the crack speed was not prescribed. This formulation related to the weak-bond fracture enabled possible the following ‘surprising phenomena’ to be revealed.

In static mode II, the strain of the crack front bond is lower than that of the next one. A consecutive quasi-static bond rupture is thus forbidden.

In static mode II, if the alternate bonds on the crack continuation inclined differently from the crack-front bond are removed, the stresses in the crack-front bond and in the other intact bonds decrease. This suggests a possibility of partial fracture where the crack breaks only the above-mentioned alternate bonds. Also, this suggests the existence of a more general *binary crack* consisting of two branches growing along the same layer with different speeds. One of these branches disintegrates the above-mentioned alternate bonds, while the other disintegrates the remaining bonds. In fact, this phenomenon is revealed in the numerical simulations.

The manifestation of the binary crack was observed in the elastic and the viscoelastic lattice strip not only for mode II, where it can exist in a wide range of initial strains, but in the case of mode I as well; however, in the latter case, it can manifest itself only in a narrow range of the initial stresses.

Mode I crack speeds in the elastic lattice strip cover the sub-Rayleigh and supersonic ranges of the speeds as well as a close vicinity of c_1 . The range between c_R and c_1 is almost completely forbidden. However, under the influence of viscosity, the forbidden crack speed ranges narrow and can disappear. Mode II binary crack speeds can exist, in addition, within the range (c_2, c_1) . These facts are in agreement with the results obtained in Slepyan (2001) for steady-state crack propagation.

The crack speeds were found to be discontinuous functions of the creep and relaxation times.

Along with this, an auxiliary problem related to a slow crack in the viscoelastic lattice was considered (as in Slepyan (2000) for a square-cell lattice). In contrast to mode I where the related auxiliary problem corresponded to the break of one bond, the mode II related auxiliary problem was considered as that for a sudden rupture of two neighboring bonds. In the creep-relaxation plane, the separation of the static amplitude response domain from the dynamic overshoot domain was performed for both modes.

Acknowledgements

This research was supported by The Israel Science Foundation, Grant No. 28/00-1, and ARO, Grant No. 41363-M.

References

- Abraham, F.F., Gao, H., 2000. How fast can cracks propagate? Phys. Rev. Lett. 84 (14), 3113–3116.
- Broberg, K.B., 1999. Cracks and Fracture. Academic Press, San Diego, London, Boston, New York, Tokyo, Toronto.
- Budiansky, B., Hutchinson, J.W., Evans, A.G., 1986. Matrix fracture in fiber-reinforced ceramics. J. Mech. Phys. Solids 34, 167–189.

- Burridge, R., Conn, G., Freund, L.B., 1979. The stability of rapid mode II shear crack with finite cohesive traction. *J. Geophys. Res.* 84, 2210–2222.
- Eatwell, G.P., Willis, J.R., 1982. The excitation of a fluid-loaded plate stiffened by a semi-infinite array of beams. *IMA J. Appl. Mech.* 29 (3), 247–270.
- Fineberg, J., Marder, M., 1999. Instability in dynamic fracture. *Phys. Rep.* 313, 1–108.
- Freund, L.B., 1979. The mechanics of dynamic shear crack propagation. *J. Geophys. Res.* 84, 2199–2209.
- Gao, H., Huan, Y., Gumbsch, P., Rosakis, A.J., 1999. *J. Mech. Phys. Solids* 47, 1941–1961.
- Gerde, E., Marder, M., 2001. Friction and fracture. *Nature* 413, 285–288.
- Kessler, D.A., 1999. Steady-state cracks in viscoelastic lattice models II. Represented in the Internet: [http://xxx.tau.ac.il/ \[Physics cond-mat/9907471\]](http://xxx.tau.ac.il/Physics%20cond-mat/9907471).
- Kessler, D.A., Levine, H., 1998. Steady-state cracks in viscoelastic lattice models. Represented in the Internet: [http://xxx.tau.ac.il/ \[Physics cond-mat/9812164\]](http://xxx.tau.ac.il/Physics%20cond-mat/9812164).
- Kessler, D.A., Levine, H., 2000. Nonlinear lattice model of viscoelastic mode III fracture. Represented in the Internet: [http://xxx.tau.ac.il/ \[Physics cond-mat/0007149\]](http://xxx.tau.ac.il/Physics%20cond-mat/0007149).
- Knauss, W.G., 1973. The mechanics of polymer fracture. *Appl. Mech. Rev.* 26, 1–17.
- Knauss, W.G., 1993. Time dependent fracture and cohesive zones. *J. Eng. Mater. Technology* 115, 262–267.
- Kulakhmetova, S.A., Saraikin, V.A., Slepyan, L.I., 1984. Plane problem of a crack in a lattice. *Mech. Solids* 19, 101–108.
- Lauterwasser, B.D., Kramer, E.J., 1979. Microscopic mechanisms and mechanics of craze growth and fracture. *Philos. Mag. A* 39, 469–495.
- Lee, O.S., Knauss, W.G., 1989. Dynamic crack propagation along a weakly bonded plane in a polymer. *Exp. Mech.* 29 (3), 342–345.
- Marder, M., Gross, S., 1995. Origin of crack tip instabilities. *J. Mech. Phys. Solids* 43, 1–48.
- Marder, M., Liu, X., 1993. Instability in lattice fracture. *Phys. Rev. Lett.* 71 (15), 2417–2420.
- Meda, G., Steif, P.S., 1994a. A detailed analysis of cracks bridged by fibers—I. Limiting cases of short and long cracks. *J. Mech. Phys. Solids* 42, 1293–1321.
- Meda, G., Steif, P.S., 1994b. A detailed analysis of cracks bridged by fibers—II. Cracks of intermediate size. *J. Mech. Phys. Solids* 42, 1323–1341.
- Movchan, N.V., Willis, J.R., 1996. Critical load for a mode-I crack reinforced by fibres. *Quart. J. Mech. Appl. Math.* 49 (4), 545–564.
- Movchan, N.V., Willis, J.R., 1997a. Asymptotic analysis of reinforcement by frictional fibres. *Proc. R. Soc. A* 453, 757–784.
- Movchan, N.V., Willis, J.R., 1997b. Influence of spatial correlations on crack bridging by frictional fibres. *Eng. Fract. Mech.* 58, 571–579.
- Movchan, N.V., Willis, J.R., 1998. Penny-shaped crack reinforced by fibres. *Quart. Appl. Math.* 56 (2), 327–340.
- Needleman, A., Rosakis, A.J., 1999. The effect of bond strength and loading rate on the conditions governing the attainment of intersonic crack growth along interfaces. *J. Mech. Phys. Solids* 47, 2411–2449.
- Nemat-Nasser, S., Luqun, N., 2001. A fiber-bridged crack with rate-dependent bridging forces. *J. Mech. Phys. Solids* 49, 2635–2650.
- Pechenik, L., Levine, H., Kessler, D.A., 2000a. Steady-state mode III cracks in a viscoelastic lattice model. Represented in the Internet: [http://xxx.tau.ac.il/ \[Physics arXiv:cond-mat/0002313\]](http://xxx.tau.ac.il/Physics%20arXiv:cond-mat/0002313).
- Pechenik, L., Levine, H., Kessler, D.A., 2000b. Steady-state mode I cracks in a viscoelastic triangular lattice. Represented in the Internet: [http://xxx.tau.ac.il/ \[Physics arXiv:cond-mat/0002314\]](http://xxx.tau.ac.il/Physics%20arXiv:cond-mat/0002314).
- Ravi-Chandar, K., Knauss, W.G., 1984. An Experimental investigation into dynamic fracture: III. On steady-state crack propagation and crack branching. *Int. J. Frac.* 26, 141–154.
- Rosakis, A.J., Samudrala, O., Singh, R.P., Shukla, A., 1998. Inter-sonic crack propagation in bimaterial systems. *J. Mech. Phys. Solids* 46, 1789–1813.
- Rosakis, A.J., Samudrala, O., Coker, D., 1999. Crack faster than the shear wave speed. *Science* 284, 1337–1340.
- Slepyan, L.I., 1981. The problem of the propagation of a cut at transonic velocity. *Sov. Phys. Dokl.* 26, 1192–1193.
- Slepyan, L.I., 1982. Antiplane problem of a crack in a lattice. *Mech. Solids* 17 (5), 101–114.

- Slepyan, L.I., 2000. Dynamic factor in impact, phase transition and fracture. *J. Mech. Phys. Solids* 48, 927–960.
- Slepyan, L.I., 2001. Feeding and dissipative waves in fracture and phase transition. III. Triangular-cell lattice. *J. Mech. Phys. Solids* 49, 2839–2875.
- Slepyan, L.I., Ayzenberg, M.V., Dempsey, J.P., 1999. A lattice model for viscoelastic fracture. *Mech. Time-Dependent Mater.* 3, 159–203.
- Willis, J.R., 1993. Asymptotic analysis of crack bridging by ductile fibres. *Composites* 24, 93–97.